ENERGY, ENVIRONMENT & STORAGE

AN INTERNATIONAL JOURNAL

Editor in Chief
Dr. Selahaddin Orhan AKANSU

# ENERGY, ENVIRONMENT AND STORAGE

EES JOURNAL

VOLUME 3, ISSUE 1, REVIEWER BOARD

AIM AND SCOPE

Energy, Environment and Storage papers consider the prospects of energy technologies, environment, materials, process control and industrial systems. The Energy, Environment and Storage will be published 3 times per year.

Contributions describe novel and significant applications to the fields of:

- Hydrogen Fuels
- Hydrogen and Fuel Cell
- Hydrogen Economic
- Biomass
- Solar PV Technology
- Solar Thermal Applications
- Wind Energy
- Materials for Energy
- Drones and Energy Applications
- Nuclear Energy and Applications
- Hydro Power
- Fuel Technologies (CNG, LNG, LPG, Diesel, Gasoline, Ethanol, etc.)
- Numerical Modelling
- Energy Storage and Systems
- Battery Technologies
- Energy Management
- Heat and Mass Transfer
- Aerodynamics
- Aerospace and Energy Applications
- Combustion
- Electric Vehicle Transportation
- Off-grid Energy Systems
- Environment Management
- Air Pollution
- Water and Wastewater Pollution
- Water and Wastewater Management
- Waste Management
- Global Warming and Climate Change
- Environmental Ecosystem
- Environmental System Modelling and Optimization
- Ecological Applications or Conservation

CONTENTS

Energy, Environment and Storage

Journal Homepage: www.enenstrg.com

Hydrogeochemical Characteristics and Groundwater Quality Assessment of a Relatively-Pristine Agricultural Basin (Palas Basin)

Ömer Karadeniz[1], Filiz Dadaser-Celik[2*]

[1] *Erciyes University, Department of Environmental Engineering, Kayseri, Türkiye, ORCID: 0000-0002-7274-9032*

[2] *Erciyes University, Department of Environmental Engineering, Kayseri, Türkiye, ORCID: 0000-0003-3623-7723*

ABSTRACT. This study investigates the spatial and temporal changes in groundwater levels and quality in the Palas Basin, a relatively-pristine semi-arid agricultural basin in Türkiye. Although groundwater is solely used as irrigation and drinking-potable water resource throughout the basin, measurements regarding the dynamics and quality of groundwater were quite rare. The analyses were based on data collected from 12 water quality monitoring wells and 15 groundwater level monitoring wells during June 2019-May 2020. Water samples were analyzed for pH, electrical conductivity, temperature, nitrate, nitrite, ammonium, total nitrogen, total hardness, alkalinity, chloride, sulfate, phosphate, total organic carbon, calcium, magnesium, sodium, potassium, and arsenic. Data analyses included hydrogeochemical analysis and multivariate statistical analysis such as principal component analysis and cluster analyses. Results showed that water quality in the basin is mostly controlled by natural factors, however, anthropogenic impacts from agriculture activities were apparent in some regions. The basin shows significant changes in water levels throughout the year due to irrigation activities. The groundwater quality was classified as either Ca-Mg-HCO$_3$ and Ca-Mg-SO$_4$ type. In the majority of the basin, water quality was suitable for irrigation and drinking water uses, however, a few sampling sites had very high electrical conductivity, sulfate, nitrate, and arsenic levels. The high levels of nitrates were detected in areas, where agriculture is intense, indicating that agricultural activities might be affecting water quality. High sulfate, electrical conductivity, and arsenic levels could be related to the hydrogeological setting of the basin. This study showed that agricultural activities and natural factors were effective on the hydrogeochemical characteristics of the Palas Basin.

1. INTRODUCTION

Groundwater is an important resource, used for meeting municipal, industrial, and agricultural water requirements, particularly when surface water resources are limited [1, 2]. The pressure on groundwater resources increases everyday due to population growth, industrial development, and agricultural intensification [3, 4]. Overexploitation and water quality deterioration are two important problems that threaten the sustainability of groundwater systems.

Groundwater is used extensively worldwide for meeting agricultural water requirements. On the global basis, the total area irrigated by groundwater is estimated to be 98 million ha or 39% of total irrigated area [5]. The amount of groundwater use is estimated to be 545 km^3 yr^{-1} [5]. As large amounts of water are extracted for irrigation, groundwater level and quality changes have been detected in many previous studies [6-8]. With the climatic changes, the pressure on groundwater systems is expected to become more apparent [6].

In this study, we collected data from a relatively pristine agricultural basin in Türkiye (Palas Basin) and analyzed the groundwater level and quality data to investigate hydrogeochemical characteristics of groundwater and spatial and temporal changes in groundwater levels and quality. In Türkiye, groundwater is used as the water resource at about 49% of total irrigated area [5]. Surface water and groundwater use in all sectors was estimated to be 54 billion m^3 yr^{-1} [9]. The amount of groundwater use in the agricultural sector was estimated as 9.8 billion m^3 yr^{-1} [9] and 9.3 billion m^3 yr^{-1} [5] by two different studies. Groundwater use is particularly important for agriculture in the semi-arid Central Anatolia region, as surface water resources are comparatively limited than other regions. Changes in groundwater levels has received significant attention in Türkiye in recent years. Downward trends in groundwater levels have been reported in different basins [10-12]. Despite strong interest in groundwater level declines, groundwater quality changes and the relationship of these changes with agricultural activities have not been sufficiently explored. Most of the basins, examined in earlier studies, were under a number of stress factors (such

as population growth, urbanization, etc.) and the relationships of water quality with agricultural activities could not be clearly established.

The main purpose of this study is to evaluate the spatial and temporal changes in groundwater levels and quality in the Palas Basin. Groundwater is used as drinking and irrigation water in the Palas Basin, where agricultural activities are common and surface waters are insufficient. There are no large cities and almost no industrial activity in the basin, therefore agriculture can be considered as one of the major drivers for groundwater quality and level changes. This study may provide insights for understanding the linkage between the agricultural activities and groundwater systems in semi-arid regions.

2. MATERIALS AND METHODS

2.1 Study Area

The study area, Palas Basin, is located in the Kayseri province, in the Central Anatolia region of Türkiye (Fig. 1). The basin is located at 1135 m (asl) altitude and has a drainage area of 480 km^2 [13]. Palas Basin, which has the characteristics of a sedimentary basin, is surrounded by hills with relative elevation differences of 300-400 m. With this feature, it is a closed basin. The central basin has a relatively low slope and the basin topography extends from east to west. Tuzla Lake is a shallow saline lake with an altitude of 1131 m, located to the northwest of the basin. Tuzla Lake, which has a length of about 8 km and a width of about 4 km, has a surface area of 35 km^2. The lake is fed by Değirmen River, springs, and groundwater [12].
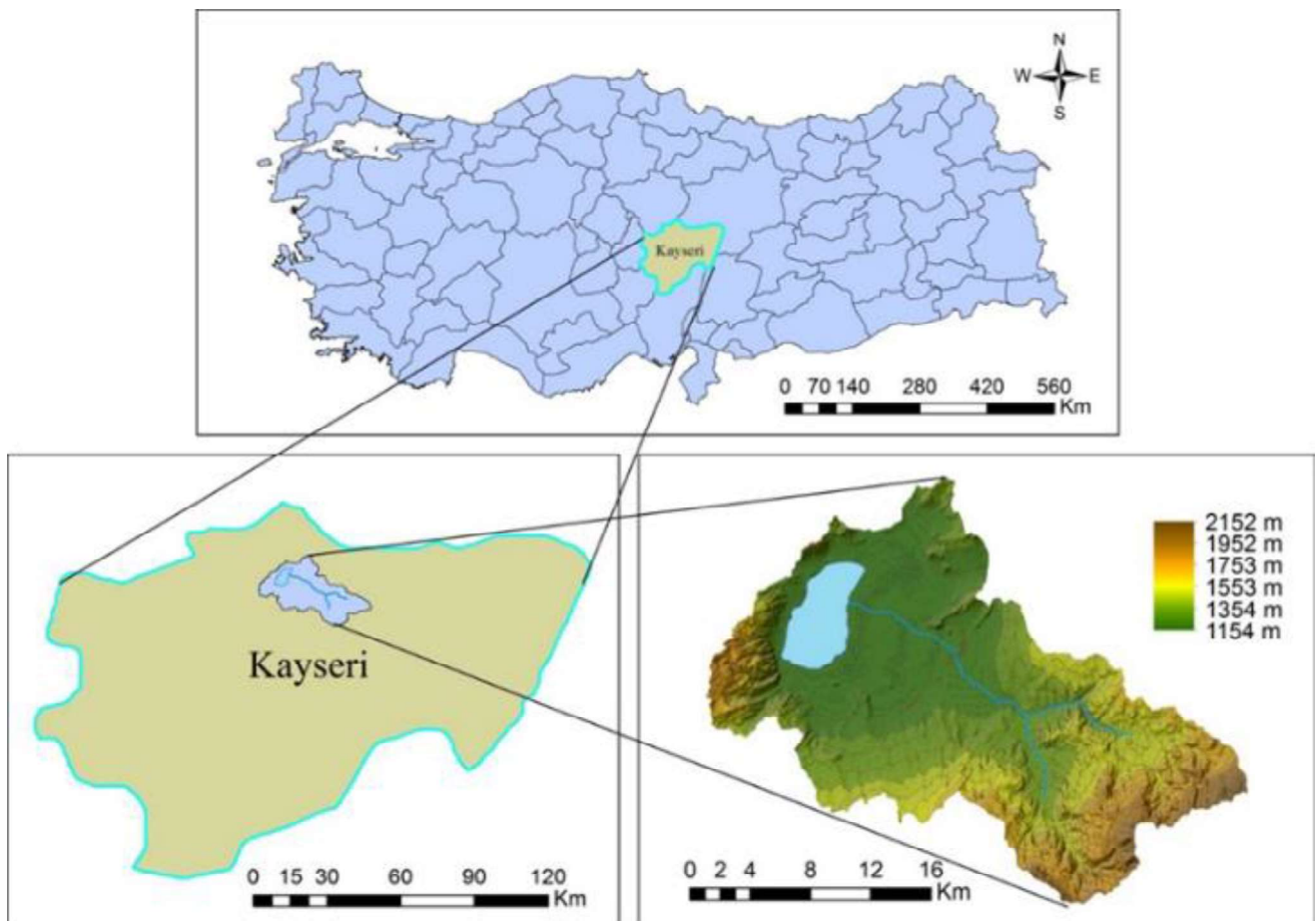
Fig. 1. Location and geographic characteristics of the Palas Basin

The study area has a semi-arid climate. Therefore, the summer months are hot and dry and it is quite cold and snowy in the winter. Average annual temperature in the region is 10.6°C (based on the 1975-2018 period). Most of the precipitation occurs in winter and spring. The average annual precipitation is 411 mm (1975-2018 average).

Geological formations in the Palas Basin can be divided into three main groups. These are Quaternary alluviums in the lake and its immediate surroundings, Tertiary-aged formations spread over a wide area in the east of the basin, and Mesozoic formations located in a narrow area in the southwest of the basin (Fig. 2). Palas Basin was formed by the filling of the quartz-aged alluvium that collapsed as a result of faulting. The oldest units in the basin are Mesozoic

units and they cover an area of approximately 33 km^2, in the southwestern part of the basin. The mountains surrounding the west of the basin are composed of ophiolitic series and these series consist of marly, sandy, and calcareous rocks with conglomerates in some places. Ophiolites in the southern mountains contain large serpentine blocks and are found in volcanics such as diorite and gabbro. Tertiary formations spread over a wide area in the east and south of the basin. Eocene flysch covers 210 km^2 of the basin, while neogene basalts, volcanics, unallocated terrestrial sediments, and conglomerates cover an area of approximately 52 km^2. Quaternary formations are the youngest units in the basin. They cover an area of approximately 148 km^2 around Tuzla Lake (Fig. 2).
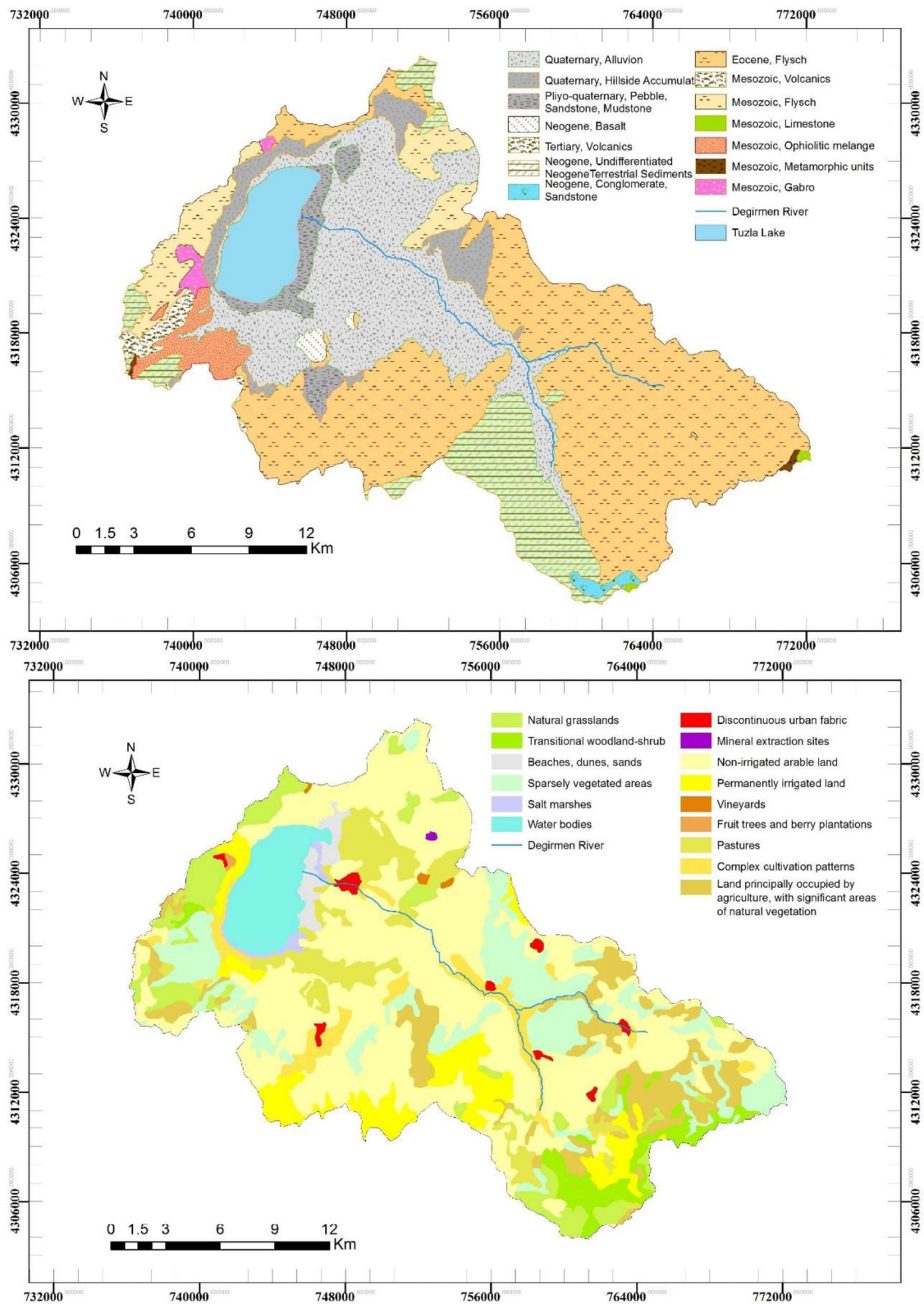
Fig. 2. Geological and land use/cover characteristics of the Palas Basin

Agriculture is the major economic activity in the study area. 60% of the basin is used as agricultural land [13](Fig. 2). Due to its distance from the city center, industry has not developed in the region. Palas Basin land cover was obtained from the CORINE 2018 database. A large part of the basin covers non-irrigated arable lands (39%), sparse vegetation (27%) and continuously irrigated areas (15%). Other important land cover classes include natural meadows (5.5%) and areas with natural vegetation (4%).

Palas Lake covers about 2% of the basin. Azgin and Dadaser-Celik [14] observed that irrigated agriculture intensified in the region, which caused further decrease in surface water flows. In another study, the changes in water levels of Tuzla Lake (Kayseri) were found to be related to groundwater level decreases [13]. The susceptibility of groundwater levels to irrigation was investigated using a groundwater flow model [12, 15]. To the best of our knowledge, no extensive analysis on groundwater quality is

available for the basin. This is very important research gap for a basin where groundwater provides the only water resource for drinking and irrigation uses.

2.2 Sample Collection and Field and Laboratory Studies

A groundwater sampling campaign was designed to determine the groundwater quality and groundwater levels in the study area. For this purpose, 12 water quality sampling wells were selected considering the locations of settlements and agricultural areas in the region (Fig. 3a). 15 sampling wells were used for monitoring groundwater levels (Fig. 3b). In order to monitor the spatial changes in groundwater quality as well as the temporal changes, samples were collected monthly from June 2019 to May 2020.

Fig. 3. Groundwater level (a) and quality (b) sampling points

Analyses for pH, electrical conductivity, temperature, nitrate (NO_3^-), nitrite (NO_2^-), ammonium (NH_4^+), total nitrogen (TN), total hardness, alkalinity, chloride (Cl^-), sulfate (SO_4^{2-}), phosphate (PO_4^{-3}), and total organic carbon (TOC) were performed monthly. Seasonal analyses were conducted for calcium (Ca^{2+}), magnesium (Mg^{2+}), sodium (Na^+), potassium (K^+), and arsenic (As^{3+}) (May 2019, July 2019, September 2019, and January/February 2020). pH, temperature, and electrical conductivity were measured on-site using Hach Lange HQ-40D multimeter. For other analyses, samples were transported to the laboratory and stored in the refrigerator at +4°C until the analysis was done. Nitrate (EN 38405 D-2), ammonium (ISO 7150-1), total nitrogen (EN ISO 11905-1), phosphate (EN ISO 6878), and sulfate (Extinction/Turbidimetric) analyses were conducted using spectrophotometric methods using Hach Lange cuvette tests. Alkalinity (SM 2320 B), hardness (SM 2340 C), and chloride (SM 4500- C1 B) were measured by titration. Calcium, magnesium, potassium, sodium, and arsenic were measured using an ICP-MS Device, while TOC was measured using a Shimadzu TOC-L CPN device.

2.3 Data Analyses

The collected water level data were used to identify seasonal changes in groundwater levels. These data were also used to identify groundwater flow direction in the center alluvial aquifer system.

Water quality data were first analyzed for seasonal variations. We also evaluated the suitability of groundwater for municipal and irrigation uses by comparing the values with limit values set by World Health Organization (WHO). Piper diagram was prepared for understanding the characteristics of the groundwater in the basin. SAR diagram was used to evaluate the suitability of waters for irrigation.

We applied multivariate statistical techniques for analyzing water quality data. Principal component analysis is a data transformation technique that converts multivariate data sets into fewer data sets, namely basic components (PC), by capturing their basic characteristics [16]. The PCs obtained rank the variation from high to low. Cluster analysis was used for grouping sampling sites with similar characteristics [17]. Hierarchical clustering analysis is the combination of clusters according to their similarity or distance (Euclid, Euclidin square, Manhattan distance, etc.) values. Dendogram is a commonly used representation. Each unit in the dendogram represents a cluster and the two closest units combine to form another cluster.

3. RESULTS AND DISCUSSION

3.1 Water Level Changes

Groundwater levels were monitored at 15 wells between June 2019 and May 2020 in the Palas Basin (Fig. 3a). We developed a map (Fig. 4) to show average groundwater levels in the region during the analysis period. In this analysis, we focused on the alluvium aquifer in the central basin, due to the presence of comparatively higher number of sampling wells in this region. As can be seen groundwater flows from southeast to the northwest and discharges in to Tuzla Lake as documented by previous studies [12].

We investigated the seasonal changes in groundwater levels from June 2019 to May 2020 (Fig. 5). The lowest value in the groundwater levels in the study area is the S8 sampling well, located at 47.5 m at 1174 m in the northeast of the basin. It was observed that groundwater levels at the majority of the wells went down during the summer and autumn seasons. The decrease in water levels could be clearly identified in sampling wells S5 and S15, which are located in the area where irrigated agriculture is concentrated. It was observed that water levels increased in

the entire basin following precipitation in the winter and spring seasons.
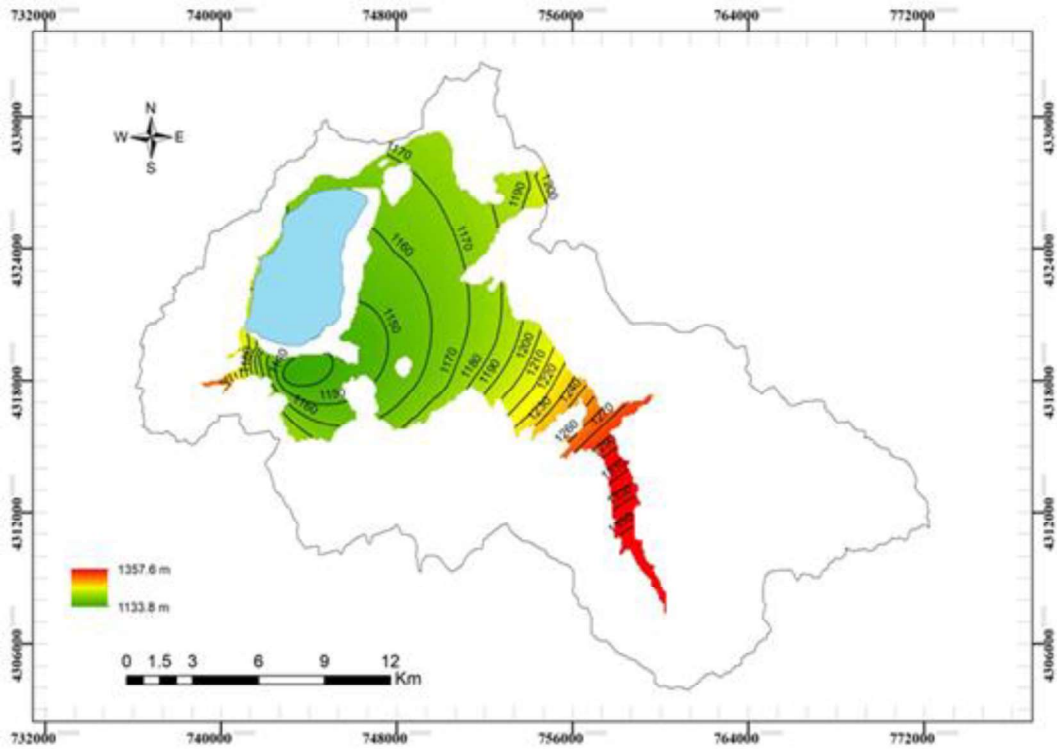
Fig. 4. Average groundwater elevations (m) during the June 2019-May 2020 period
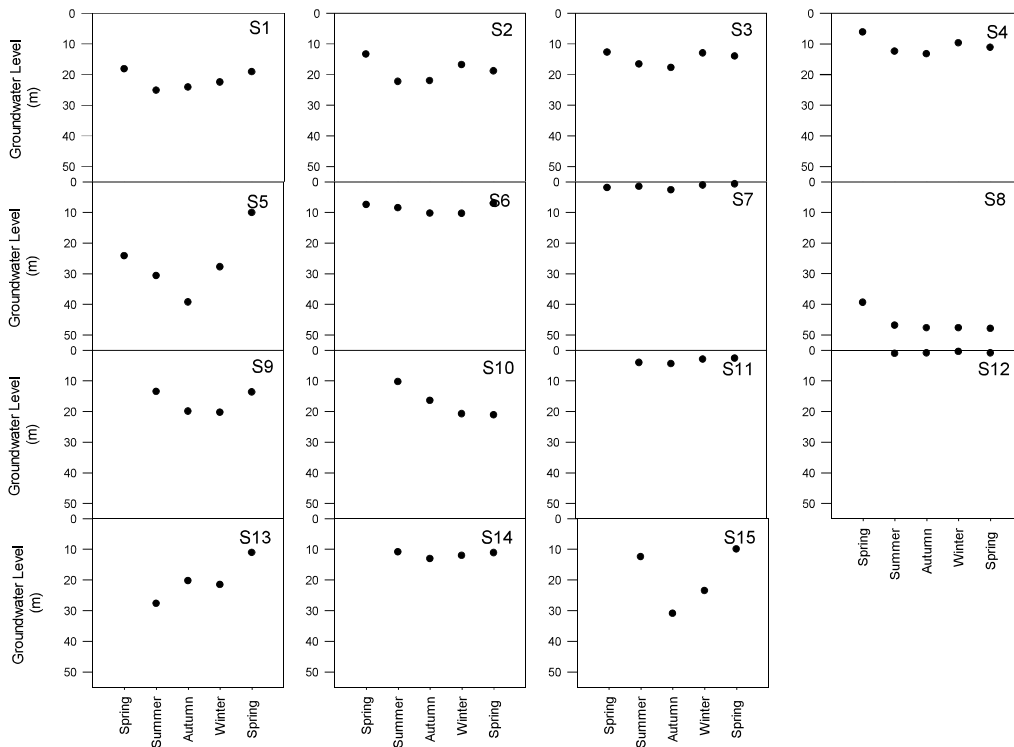
Fig. 5. Seasonal changes in groundwater levels during the June 2019-May 2020 period

3.2 Hydrogeochemical Characteristics and Suitability of Groundwater for Drinking Water Uses

Groundwater quality varies as a result of natural factors as well as anthropogenic activities [4, 18, 19]. The hydrogeochemical characteristics of groundwater are related to the soil/bedrock material, the residence time in

the aquifer, and biological and chemical processes [20]. Investigating the chemical composition of groundwater can improve our understanding of these processes and help identify the sources of pollution [21, 22]. Averages of monthly measurements collected in the Palas Basin are given in Table 1. Spatial distribution of average values is given in Fig. 6. The suitability of groundwater quality as drinking water was evaluated according to the limit values set by the World Health Organization (WHO).

Table 1. Average groundwater quality values (June 2019 - May 2020) (BL: below detection limit)

Sample No	K1	K2	K3	K4	K5	K6	K7	K8	K9	K10	K11	K12
Temperature (°C)	18.2	16.5	16.5	14.2	14.9	17.1	17	22.5	16.2	16.8	17.2	17.9
pH	8.2	7.8	8.2	7.9	7.9	8.1	8	8.1	8	8.2	8.1	8.1
Electrical Conductivity (µs/cm)	1009	1757	1681	714	666	388	350	570	461	558	371	2134
Nitrate (mg/L)	18	18	17	59	65	9	10	21	15	27	11	26
Ammomium (mg/L)	0.2	0.1	0.1	0.1	0.1	0.05	0.1	0.2	0.1	0.2	0.4	0.1
Total Nitrogen (mg/L)	6.4	5.8	7.4	13.5	20.2	3.2	4.3	6.2	4.9	7.5	5.2	6.9
Hardness (mg/L)	463	927	1002	330	252	191	175	258	252	276	195	1341
Phosphate (mg/L)	0.2	0.4	BL	BL	0.1	BL	BL	0.6	BL	0.1	0.5	D
TOC (mg/L)	0.7	1.3	1.5	2.1	1.8	0.5	0.5	0.7	0.6	0.5	0.5	0.9
Arsenic (mg/L)	0.06	BL	0.02	BL	0.01	0.05	0.01	0.61	0.01	BL	0.03	0.01
Calcium (mg/L)	62	128	63	25	24	9	46	12	9	29	12	88
Magnesium (mg/L)	127	137	121	107	59	52	40	54	83	51	44	137
Sodium (mg/L)	12.4	19.1	13.3	7.8	8.4	5.3	2.9	6.1	3.6	3.2	3.7	15.2
Potassium (mg/L)	6.5	3.1	3.8	4.3	2.5	1.4	1.6	1.1	2.7	2	1.8	1
Sulfate (mg/L)	32	809	896	57	49	35	13	19	13	18	5	1188
Chloride (mg/L)	139	50	72	27	41	13	12	35	16	22	17	49
Bicarbonate (mg/L)	271	194	168	271	247	203	182	231	234	248	189	104

According to the analysis conducted between June 2019 and May 2020, the average temperature values range between 14 °C and 22.5 °C in twelve monitoring wells. K8 interestingly has higher water temperatures than other locations. K8 is located close to the Tuzla Lake. We can speculate that there is an interaction between the well and surface water body, which created higher water temperatures [23].

The pH is calculated by taking the logarithm of the hydrogen ions in the solution and indicates the acidic or basic state of the solution. As a result of year-round analysis, average pH values were between 7.8 and 8.2, indicating almost neutral conditions. At all sampling points, it was between 6.5-8.5, which is pH range proposed by the WHO, for water to be used as drinking water.

The average electrical conductivity values changed between 371 and 2134 µS/cm. Electrical conductivity values increased during the summer months, most probably due to the reduction in groundwater recharge and decrease in groundwater levels, which concentrate the ions [20]. It was observed that the sampling points, K1, K2, K3, and K12, had electrical conductivity values higher than other sampling points. Electrical conductivity consists of ions dissolved in water and is an important parameter for determining water use for different purposes. In general, water quality is classified as 'good' when electrical conductivity values are between 250 and 750 µS/cm [24]. The electrical conductivity limit value determined by the WHO for drinking water is 2500 µS/cm. In this study, it was determined that all sampling wells had electrical conductivity values below the limit value set by WHO. However, in some stations the electrical conductivity values were higher than 750 µS/cm.

Nitrate is the most common type of pollutant in groundwater systems [25]. Fertilizers used in agriculture contain nitrate, ammonium, and organic nitrogen, and their excessive use causes nitrogen pollution due to mixing of agricultural drainage with groundwater [26]. The average value in nitrate measurements varied between 9-65 mg/L. Average values in ammonium measurements were in the range of 0.05-0.4 mg/L. While the nitrate limit value determined by the WHO for drinking water is 50 mg/L, the ammonium limit value is determined as 1.5 mg/L. Total nitrogen was in the range of 3.2 mg/L and 20.2 mg/L. Of the sampling wells, only the nitrate values measured at K4 and K5 wells exceeded the limit value of 50 mg/L. In terms of ammonium, all sample wells had ammonium concentrations below the limit value. Sampling wells with high nitrate levels were generally located at areas where agriculture and animal husbandry are common. Also the water levels in these wells are closer to the land surface, which may be increasing the risk for contamination.

The excessive use of fertilizers in agriculture causes phosphate to be adsorbed in the soil and can be mixed with groundwater after rainfall [27]. Average values in phosphate rise up to 0.6 mg/L. There is no limit value for any phosphate determined by the WHO for drinking water.

TOC originates from organic substances dissolved in water or synthetic waste from homes and industrial facilities. The average value in TOC measurements ranges from 0.5 to 2.1 mg/L. There is no TOC limit value determined by the WHO for drinking water. However, high TOC values can create a problem during chlorination as they increase the potential for trihalomethane formation [28].

The average arsenic measurements were smaller than 0.61 mg/L. The primary source of arsenic is volcanic rocks. The limit value determined by the WHO for drinking water is 0.01 mg/L. Erciyes Mountain, a volcanic mountain about 50 km away from the basin, can be associated with the amount of arsenic in the region. Similar to our study, a

previous study, conducted in the same region, identified
high arsenic concentrations [29].
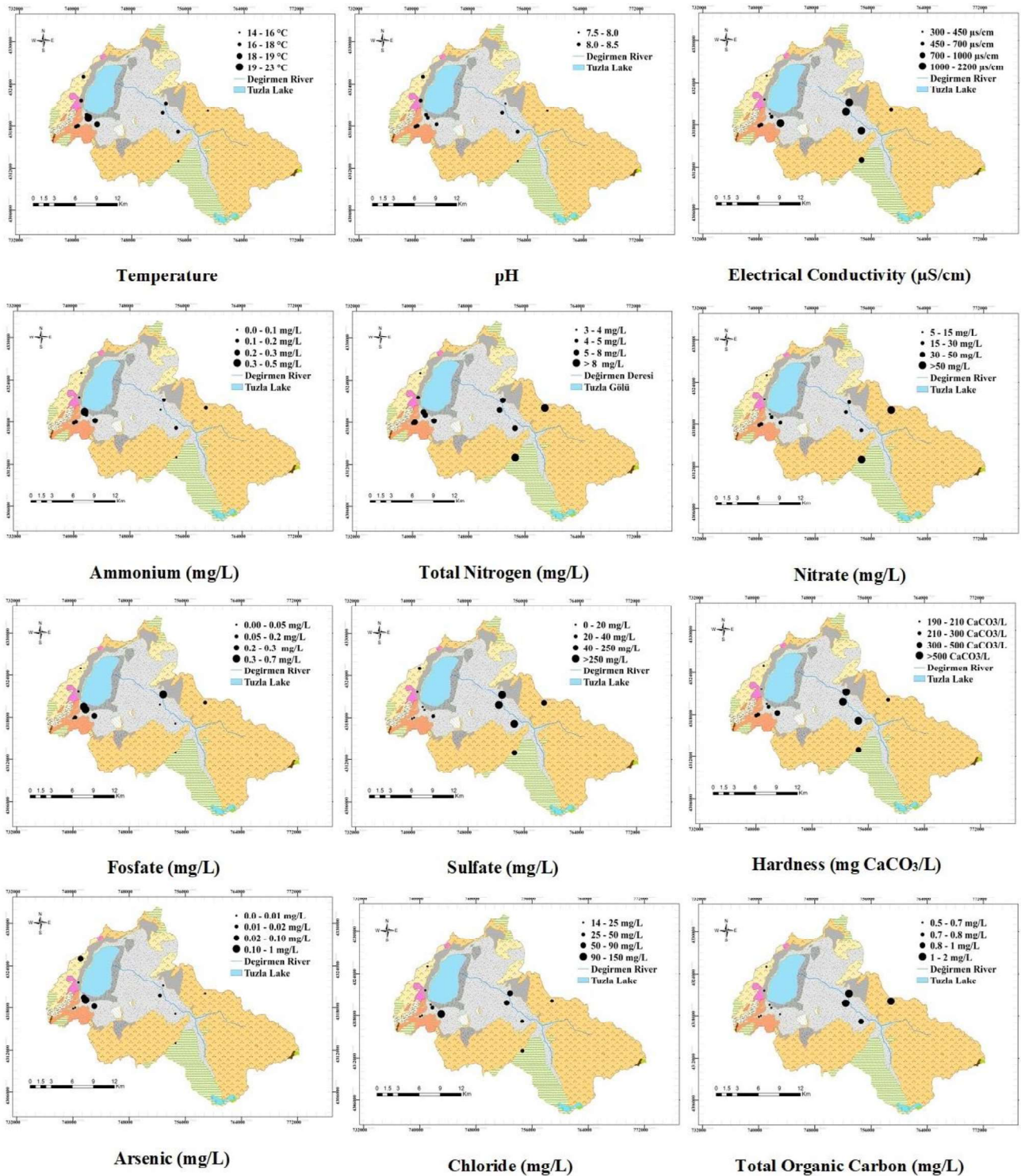
Fig. 6. Average values of water quality parameters

Major cations in groundwater were sodium, calcium, magnesium and potassium and major anions were chloride, bicarbonate, and sulfate (Table 2). Average concentrations of cations were in order magnesium>calcium>sodium> potassium for almost all sampling sites, while for the anions the order is as bicarbonate>chloride>sulfate for K1, K8, K9, K10, and K11 and bicarbonate>sulfate>chloride for

K4, K5, K6, and K7. K2, K3, and K12 have completely different characteristics in terms of anions. In these sites, the anion concentrations are in order as sulfate>bicarbonate>chloride. Magnesium is the dominant cation, present at concentrations range from 40 mg/L to 137 mg/L. Sulfate is the dominant anion in sampling sites, K2, K3, and K12; and bicarbonate is the dominant one in others. The concentrations of calcium and magnesium, which are multivalent (+2) cations, form hardness of water, changed between 195 and 1341 mg CaCO$_3$/L. Rock types such as calcite and dolomite contain calcium and magnesium [30]. The low amount of calcium and magnesium in drinking water can negatively affect bone development in children, while high concentrations can cause kidney stone formation, and arthritis problems [31, 32]. The hardness limit value determined by the WHO for drinking water is 500 mg CaCO$_3$/L. Sampling points other than K2, K3, and

K12, had hardness values below this limit value. According to the "French hardness" value, K1, K2, K3, K4, and K12 wells had waters in the "very hard water" class, while the others had waters in the "hard water" class.

3.3 Correlation Analysis

We conducted correlation analysis for understanding the relationships between different water quality parameters. In this analysis, we calculated Spearman correlation coefficient. The results (Table 2) showed that electrical conductivity is strongly and positively correlated with calcium (r = 0.85), magnesium (r = 0.87), sodium (r = 0.92), and sulfate (r = 0.96). This shows that aquifer chemistry is generally controlled by these ions. We also determined a strong and positive correlation between the ions sodium +, sulfate (r = 0.81), and chlorine (r = 0.61).

Table 2. Correlation matrix of the 10 hydrogeochemical variables

Parameter	pH	EC	NO$_3^-$	Ca^{2+}	Mg^{2+}	Na$^+$	K$^+$	SO$_4^{2-}$	Cl$^-$	HCO$_3^-$
pH										
EC	-0.03									
NO$_3^-$	-0.44	0.01								
Ca^{2+}	-0.24	0.85	-0.11							
Mg^{2+}	-0.11	0.87	0.09	0.77						
Na$^+$	-0.22	0.92	0.08	0.89	0.89					
K$^+$	0.04	0.16	0.19	0.24	0.55	0.36				
SO$_4^{2-}$	-0.02	0.96	-0.09	0.79	0.74	0.81	-0.06			
Cl$^-$	0.32	0.48	-0.00	0.46	0.65	0.61	0.77	0.26		
HCO$_3^-$	-0.11	-0.58	0.41	0-.45	-0.22	-0.34	0.53	-0.76	0.15	

3.4 Classification of Groundwater and Suitability of Groundwater for Irrigation

The Piper diagram is commonly used in water chemistry analysis is shown in Fig. 7. The Piper diagram allows the evaluation of the hydrogeochemical types of water based on the anion and cation concentrations [33]. The diagram consists of three main regions. While the regions with equilateral triangles are composed of anions and cations, the diamond structure consists of two triangles. When the triangle with cations was examined in all sample wells, it was seen that while the triangle with the anions was "Magnesium type", the K2, K3, and K12 sample wells were "Sulfate type" waters and the remaining sample wells were in the "bicarbonate type" class. Looking at the diamond structure, it is seen that the dominant water type in the Palas Basin is "Calcium-Magnesium-Bicarbonate type" waters,

while K2, K3, and K12 sampling wells are "Calcium-Magnesium-Sulfate type" waters. This can be due to the dissolution of carbonate and gypsum, calcite, and anhydrite in groundwater [34].

Sodium adsorption rate (SAR) and electrical conductivity show the probability of waters in agriculture according to the electrical conductivity and SAR ratio with the US salinity diagram [35] (Fig. 7). In Fig. 7, C1, C2, C3, C4 are located next to S1, S2, S3, S4, K1, K2, K3, K12 high saline and low sodium (C3-S1) class waters, which represent medium, high, and very salty waters. All remaining sample wells were classified as medium saline and low sodium (C2-S1) class waters. While C2-S1 class waters can be used for irrigation for salt-resistant plants, C3-S1 class waters can be used for medium and high salt-resistant plants.
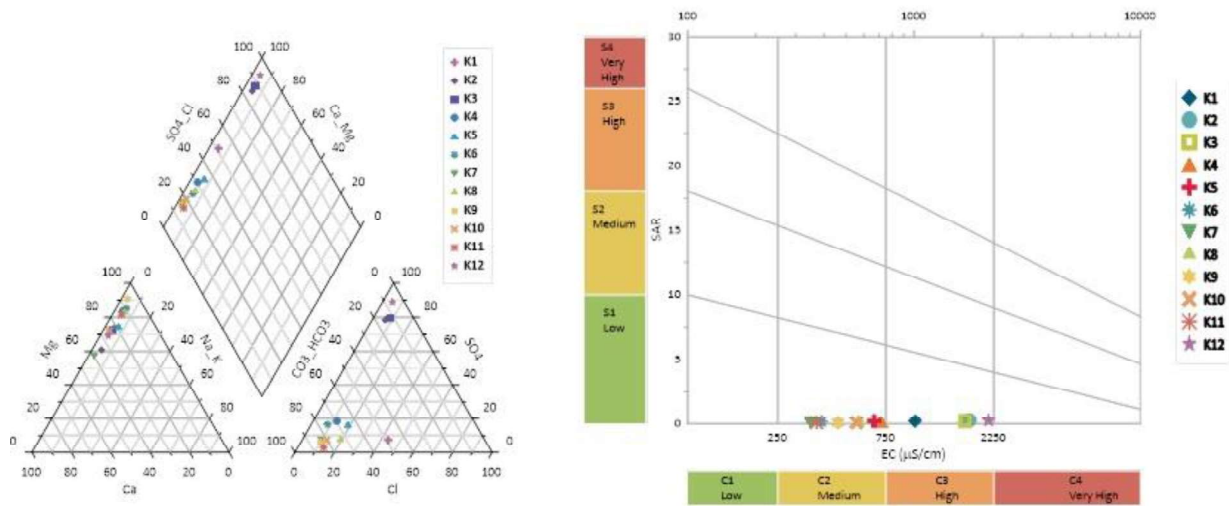
Fig. 7. Piper diagram and U.S. salinity diagram

3.5 Principal component analysis (PCA)

PCA analysis was performed by including 17 parameters (pH, temperature, electrical conductivity, sodium, calcium, magnesium and potassium and major anions were chloride, bicarbonate, sulfate, nitrate, ammonium, TN, TOC, Arsenic, hardness, phosphate). The analysis was conducted using IBM SPSS Statistics Base 22.0. PCA separated the chemical variables into four orthogonal main components (PC1, PC2, PC3, PC4). The total variance of the data matrix was 85.39%. PC1 explained 37.31% of the total variance and is associated with electrical conductivity, sodium, hardness, magnesium, sulfate, and calcium. PC2, in which nitrate, TN, temperature, TOC, and pH contribute, explained 23.584% of the total variance. PC3 explains 13.96% of the variance and affected by chlorine, bicarbonate and ammonium, and finally PC4 is contributed by arsenic and phosphate, with 10.4% of the variance. The eigenvalues obtained as a result of PC1 to PC4 were 6.342, 4.009, 2.373, and 1.792, respectively. PC1 and PC3 appear to be mainly due to the dissolution of geological compounds. Contribution from human pollution sources appear in PC2 and PC4 with nitrate and phosphate (Table 3).

Table 3. Factor loadings

Parameter	Component			
	1	2	3	4
Electrical Conductivity	0.957	0.228	-0.005	0.109
Sodium	0.939	0.097	0.217	0.143
Hardness	0.924	0.296	-0.106	0.084
Magnesium	0.920	0.016	0.234	-0.123
Sulfate	0.889	0.306	-0.243	0.152
Calcium	0.871	0.213	0.022	0.036
Nitrate	0.130	-0.844	0.142	0.363
Total Nitrogen	0.127	-0.821	0.169	0.346
Temperature	-0.231	0.776	0.361	0.314
TOC	0.496	-0.731	0.131	0.316
pH	-0.181	0.529	0.203	-0.480
Chlorine	0.522	0.094	0.724	-0.340
Potassium	0.340	-0.355	0.664	-0.522
Bicarbonate	-0.442	-0.565	0.591	-0.147
Ammonium	-0.413	0.335	0.413	0.039
Arsenic	-0.350	0.410	0.433	0.568
Phosphate	-0.232	0.428	0.537	0.546

3.6 Hierarchical Cluster Analysis of Groundwater

Hierarchical clustering was performed using the Ward's method on 17 variable parameters obtained for 12 sample points. The analysis was conducted with Minitab 19. The difference between clusters was determined using the Euclidean distance method. The dendogram in Fig. 8 was obtained by applying the normalization process on the parameters. According to the results, 12 sample wells were divided into 3 clusters (Fig. 8).
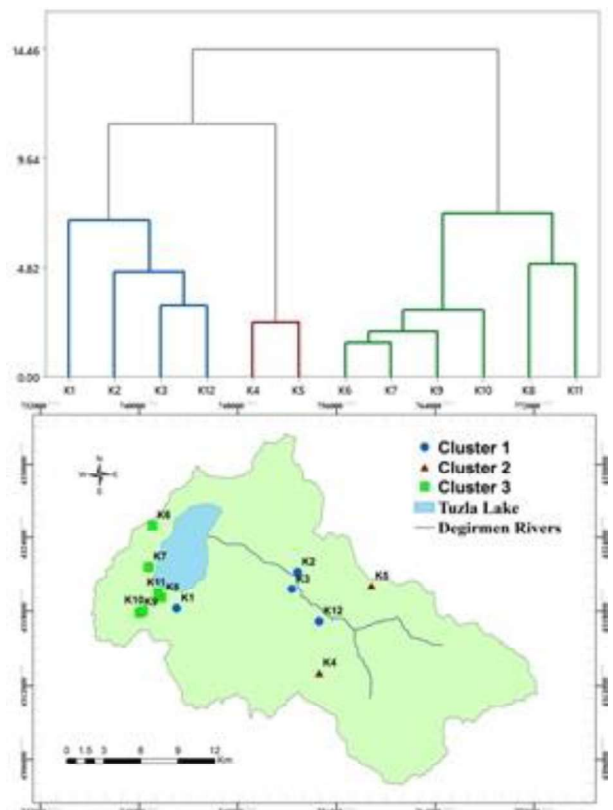
Fig. 8. Dendrogram showing clustering of sampling wells according to groundwater quality characteristics of the Palas Basin and map showing the distribution of clusters

According to the cluster analysis result conducted according to Ward's hierarchical method, K2, K3, and K12 sampling points in the center of the Palas Basin and K1 sampling wells located in the west of the basin are located in the first cluster, while K4 and K5 sampling stations are in the second cluster group. All sampling wells are included in cluster 3, except for the K1 sampling well located to the west of the Palas Basin.

4. CONCLUSIONS

Palas Basin is a small basin located in semi-arid climatic setting. The basin is a closed basin and affected only by agriculture related impacs. The general groundwater flow in the region appears to be towards the northwest. The water level in the groundwater level measurement wells varies between 0.5 m and 47.5 m from the surface. During the summer and autumn seasons, there was a serious decrease in the water levels in the wells in the region where irrigated agriculture is carried out intensively.

It was observed that the main source of pollution affecting the groundwater quality in the study area is composed of hydrogeological processes. According to the Piper Diagram, groundwater is generally located in the Calcium-Magnesium-Bicarbonate and Calcium-Magnesium-Sulfate water facies. Sulfate levels in 3 wells (K2, K3, and K12) in the basin center exceed the limit value of 250 mg/L and are considered as "sulfate type" waters. Volcanic rocks in the region cause significant arsenic pollution in some locations. At the same time, the presence of rocks such as limestone and dolomite in the region was found to increase the calcium and magnesium concentrations in the groundwater. In terms of nitrate, except for K4 and K5 wells, the limit value of 50 mg/L was not exceeded. High phosphate values in these regions indicate that there may be a pollution caused by agriculture.

REFERENCES
[1] V. Re, G. Zuppi, Influence of precipitation and deep saline groundwater on the hydrological systems of Mediterranean coastal plains: a general overview, *Hydrological sciences journal*, 56 (2011) 966-980.
[2] S. Kammoun, R. Trabelsi, V. Re, K. Zouari, J. Henchiri, Groundwater quality assessment in semi-arid regions using integrated approaches: the case of Grombalia aquifer (NE Tunisia), *Environmental monitoring and assessment*, 190 (2018) 87.
[3] R. Paul, K. Brindha, G. Gowrisankar, M.L. Tan, M.K. Singh, Identification of hydrogeochemical processes controlling groundwater quality in Tripura, Northeast India using evaluation indices, GIS, and multivariate statistical methods, *Environmental Earth Sciences*, 78 (2019) 470.
[4] R. Avtar, P. Kumar, A. Surjan, L. Gupta, K. Roychowdhury, Geochemical processes regulating groundwater chemistry with special reference to nitrate and fluoride enrichment in Chhatarpur area, Madhya Pradesh, India, *Environmental earth sciences*, 70 (2013) 1699-1708.
[5] S. Siebert, J.J. Burke, J.M. Faurès, K. Frenken, J. Hoogeveen, P. Döll, F.T. Portmann, Groundwater use for irrigation - a global inventory, *Hydrology and Earth System Sciences*, 14 (2010) 1863-1880.
[6] S. Dangar, A. Asoka, V. Mishra, Causes and implications of groundwater depletion in India: A review, *Journal of Hydrology*, 596 (2021) 126103.
[7] H. Jia, H. Qian, L. Zheng, W. Feng, H. Wang, Y. Gao, Alterations to groundwater chemistry due to modern water transfer for irrigation over decades, *Science of The Total Environment*, 717 (2020) 137170.
[8] A. Pulido-Bosch, J.P. Rigol-Sanchez, A. Vallejos, J.M. Andreu, J.C. Ceron, L. Molina-Sanchez, F. Sola, Impacts of agricultural irrigation on groundwater salinity, *Environmental Earth Sciences*, 77 (2018) 197.
[9] M. Cetin, Agricultural Water Use, in: N.B. Harmancioglu, D. Altinbilek (Eds.) *Water Resources of Turkey*, Springer International Publishing, Cham, 2020, pp. 257-302.
[10] DSİ, *Turkey Water Report 2009*, in, Devlet Su İşleri, Ankara, 2009.
[11] S. Ekercin, E. Sertel, F. Dadaser-Celik, S. Durduran, Investigating the Climate Change Impacts on the Water Resources of the Konya Closed Basin Area (Turkey) Using Satellite Remote Sensing Data, in: İ. Dincer, C.O. Colpan, F. Kadioglu (Eds.) *Causes, Impacts and Solutions to Global Warming*, Springer Science+Business Media, New York, 2013.
[12] F. Dadaser-Celik, M. Celik, Modelling surface water-groundwater interactions at the Palas Basin (Turkey) using FREEWAT, *Acque Sotterranee - Italian Journal of Groundwater*, 6 (2017) 53-60.
[13] S.T. Azgin, F. Dadaser-Celik, Spatial and temporal changes at Tuzla (Palas) Lake in Turkey, *Journal of Water and Climate Change*, 6 (2015) 787-799.
[14] S.T. Azgin, F. Dadaser-Celik, Evaluating Surface Runoff Responses to Land Use Changes in a Data Scarce Basin: a Case Study in Palas Basin, Turkey, *Water Resources*, 47 (2020) 828-834.
[15] G. De Filippis, C. Pouliaris, D. Kahuda, T.A. Vasile, V.A. Manea, F. Zaun, B. Panteleit, F. Dadaser-Celik, P. Positano, M.S. Nannucci, M. Grodzynskyi, A. Marandi, M. Sapiano, I. Kopač, A. Kallioras, M. Cannata, Y. Filiali-Meknassi, L. Foglia, I. Borsi, R. Rossetto, Spatial Data Management and Numerical Modelling: Demonstrating the Application of the QGIS-Integrated FREEWAT Platform at 13 Case Studies for Tackling Groundwater Resource Management, *Water*, 12 (2020).
[16] B. Helena, R. Pardo, M. Vega, E. Barrado, J.M. Fernandez, L. Fernandez, Temporal evolution of groundwater composition in an alluvial aquifer (Pisuerga River, Spain) by principal component analysis, *Water Research*, 34 (2000) 807-816.
[17] M. Vega, R. Pardo, E. Barrado, L. Debán, Assessment of seasonal and polluting effects on the quality of river water by exploratory data analysis, *Water Research*, 32 (1998) 3581-3592.
[18] T. Subramani, N. Rajmohan, L. Elango, Groundwater geochemistry and identification of hydrogeochemical processes in a hard rock region, Southern India,

Environmental monitoring and assessment, 162 (2010) 123-137.

[19] R. Chatterjee, G. Tarafder, S. Paul, Groundwater quality assessment of Dhanbad district, Jharkhand, India, *Bulletin of engineering geology and the environment*, 69 (2010) 137-141.

[20] L. Kiewiet, J. von Freyberg, H.J. van Meerveld, Spatiotemporal variability in hydrochemistry of shallow groundwater in a small pre-alpine catchment: The importance of landscape elements, *Hydrological Processes*, 33 (2019) 2502-2522.

[21] S. He, J. Wu, Hydrogeochemical characteristics, groundwater quality, and health risks from hexavalent chromium and nitrate in groundwater of Huanhe Formation in Wuqi county, northwest China, *Exposure and Health*, 11 (2019) 125-137.

[22] M. Tomlinson, A.J. Boulton, Ecology and management of subsurface groundwater dependent ecosystems in Australia–a review, *Marine and Freshwater Research*, 61 (2010) 936-949.

[23] J. Ren, J. Cheng, J. Yang, Y. Zhou, A review on using heat as a tool for studying groundwater–surface water interactions, *Environmental Earth Sciences*, 77 (2018) 756.

[24] K. Prakash, R. Somashekar, Groundwater quality-Assessment on Anekal Taluk, Bangalore Urban district, India, *Journal of Environmental Biology*, 27 (2006) 633-637.

[25] V. Goldberg, Groundwater pollution by nitrates from livestock wastes, *Environmental Health Perspectives*, 83 (1989) 25-29.

[26] I. Marinov, A.M. Marinov, A coupled mathematical model to predict the influence of nitrogen fertilization on crop, soil and groundwater quality, *Water resources management*, 28 (2014) 5231-5246.

[27] O.K. Borggaard, C. Szilas, A.L. Gimsing, L.H. Rasmussen, Estimation of soil phosphate adsorption capacity by means of a pedotransfer function, *Geoderma*, 118 (2004) 55-61.

[28] N. Ates, S.S. Kaplan-Bekaroglu, F. Dadaser-Celik, Spatial/temporal distribution and multi-pathway cancer risk assessment of trihalomethanes in low TOC and high bromide groundwater, *Environmental Science: Processes & Impacts*, 22 (2020) 2276-2290.

[29] C. Simsek, Assessment of naturally occurring arsenic contamination in the groundwater of Sarkisla Plain (Sivas/Turkey), *Environmental Earth Sciences*, 68 (2013) 691-702.

[30] S. Sargazi, M. Mokhtari, M.H. Ehrampoush, S.A. Almodaresi, H. Sargazi, M. Sarhadi, The application of geographical information system (GIS) approach for assessment of groundwater quality of Zahedan city, Sistan and Baluchestan Province, Iran, *Groundwater for Sustainable Development*, (2020) 100509.

[31] Y. Huang, X. Ma, Y. Tan, L. Wang, J. Wang, L. Lan, Z. Qiu, J. Luo, H. Zeng, W. Shu, Consumption of very low Mineral water is associated with lower bone mineral content in children, *The Journal of nutrition*, 149 (2019) 1994-2000.

[32] F. Kozisek, Regulations for calcium, magnesium or hardness in drinking water in the European Union member states, *Regulatory Toxicology and Pharmacology*, 112 (2020) 104589.

[33] A.M. Piper, A graphic procedure in the geochemical interpretation of water-analyses, *Eos, Transactions American Geophysical Union*, 25 (1944) 914-928.

[34] F. Ehya, Z. Marbouti, Hydrochemistry and contamination of groundwater resources in the Behbahan plain, SW Iran, *Environmental Earth Sciences*, 75 (2016) 455.

[35] L.A. Richards, *Diagnosis and improvement of saline and alkali soils*, LWW, 1954.

Energy, Environment and Storage
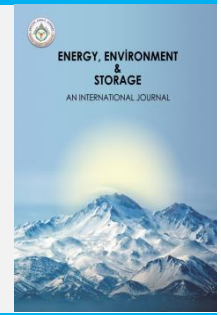
Experimental Investigation of the Effect of Acetone Additive to Diesel Fuel on Engine Performance and Exhaust Emissions at Partial Loads

Ahmet Duhan Coşkun [1], Volkan Sabri Kül [2*], Selahaddin Orhan Akansu [3]

[1*]*Erciyes University, Faculty of Engineering, Department of Mechanical Engineering, Kayseri, Turkey*
ahmetduhancoskunn@gmail.com, ORCID: 0000-0003-2529-4183

[2]*Erciyes University, Faculty of Engineering, Department of Mechanical Engineering, Kayseri, Turkey*
volkanskul@gmail.com, ORCID: 0000-0002-6412-6062

[3]*ErciyesUniversity, Faculty of Engineering, Department of Mechanical Engineering, Kayseri, Turkey*
akansu@erciyes.edu.tr, ORCID: 0000-0002-0085-7915

ABSTRACT. In this study, it is aimed to gain good characteristics that can directly affect daily life with more environmentally friendly, economical and performance fuels. For these purposes, acetone has been added to the fuel. Since acetone has a high vapor pressure, it is aimed to increase engine performance by taking advantage of its volatility. It is thought that emissions will also improve with increased engine performance. The experiments were carried out using a heavy-duty engine with a displacement of 11.670 cc. Engine performance and emission values were investigated at 100, 200 and 300 Nm partial loads and at 600 rpm constant engine speed by adding 5% and 10% acetone to diesel fuel. The results were compared with pure diesel fuel. Compared to the pure diesel fuel, the BTE value of A5D95 fuel was observed to be 3.28% and 2.60% better, respectively, under 100 and 200 Nm load, while the BTE value of A10D90 fuel was 0.23% and 0.05% worse. Compared to the pure diesel fuel, the BTE value of A5D95 fuel was observed to be 3.28% and 2.60% better, respectively, under 100 and 200 Nm load, while the BTE value of A10D90 fuel was 0.23% and 0.05% worse. Since there was an unexpected decrease in the BTE value of pure diesel under 300 Nm load, only A5D95 and A10D90 fuels were compared at this load. It was found that the BTE value of A5D95 fuel under 300 Nm load was 0.65% higher than A10D90 fuel. While 10% acetone additive A10D90 fuel could not have a positive effect on efficiency, it was determined that A5D95 fuel with 5% acetone additive was more efficient than other fuel types at all loads. When the emission rates of D100, A5D95 and A10D90 fuels are evaluated according to the power they produce under 100, 200 and 300 Nm loads, the CO emission rate of A5D95 fuel is less than that of pure diesel at other loads except 100 Nm load. However, the NO_x ratio was higher at all loads. These results support the higher efficiency of A5D95 fuel compared to pure diesel. Other results are discussed in detail in section 3.

1. INTRODUCTION

Energy consumption is a big part of our daily lives. With the increasing population, our energy needs are increasing day by day. The most commonly used source of energy consumption is fossil fuels. According to the 2020 data, fossil fuels are used at a rate of 79.3%. Petrol is the most consumed energy among fossil fuels. In 2020, oil was one of the most consumed energy sources in the world's primary energy consumption with 31.2 million % TEP. In Turkey, crude oil has been the most consumed energy source with 29 million % TEP in primary energy consumption. The transportation sector, where engines are used a lot, has a primary energy consumption of 23.42% across Turkey. Oil consumption has increased by 6% in

the world and 44% in Turkey in the last decade [1]. Diesel engines are superior to petrol engines in terms of exhaust emission and engine performance [2]. Although diesel engines have lower exhaust emissions than other engines, they still emit large amounts of gases that are harmful to the atmosphere. In order to reduce the negative effects of diesel engines and to increase engine performance, additives are used for diesel fuels. While trying to achieve higher engine performance with these additives, it is also aimed to reduce exhaust emission values. Additives may have different chemical contents. In diesel fuels formed with a titanium mixture, the engine performance has not changed much, while the exhaust emission values have been reduced [3]. Addition of less than 15% dimethyl

*Corresponding author: volkanskul@gmail.com

ether to diesel fuel reduces specific fuel consumption, while high proportions of dimethyl ether mixture increases specific fuel consumption [4]. Another study 20% LPG was used as a fuel additive, certain improvements were observed in fuel consumption and emissions [5].

In this study, acetone (C3H6O, Dimethyl Ketone) with a purity rate of 99.5% was used as an additive. Acetone is used in the production of many chemicals in the industrial sector, as a paint thinner in the paint sector, as a nail polish remover in the cosmetics sector and in the production of cleaning materials. Acetone is an extremely flammable substance [6]. According to some, while this feature is dangerous, it has the opportunity to be used as a fuel additive thanks to its highly flammable feature. Thanks to this opportunity, it is aimed to decrease the exhaust emissions compared to pure diesel and to decrease the harmful gases released to the environment. In addition, the engine performance was also requested to increase. In the study, this opportunity was evaluated by mixing 5% and 10% acetone in the rate of pure diesel mass to diesel fuel. Engine performances and exhaust emissions were measured at 100 Nm, 200 Nm and 300 Nm in the engine with these mixtures set at constant speed. The information obtained was compared with the information obtained by going through the same experimental stages of pure diesel fuel.

2. MATERIALS AND METHODS

2.1 Experimental Setup

The test setup consists of fuel, engine, engine performance test system, emission measurement system and in-cylinder pressure measurement system. Before starting the work, the cables to the systems were checked. In order to obtain more accurate and precise results, the fuel in the engine was removed from the engine without pumping new fuel into the engine.

The BOSCH BEA060 model emission analyzer was used for exhaust emissions. The emission analyzer was directly connected to a screen and
processed the emission values instantly. Instant performance information of the engine used in the experiment was obtained with the PCS Engine Test System. Another instrument used in the experiment is the PCB Piezotronics 113B22 branded piezoelectric sensor. The pressure inside the cylinder was measured with this sensor.

2.2 Fuels and Test Engine

Pure diesel (D100) and diesel-acetone mixture was used in the study. The acetone used in the experiment has 99.5% purity. The properties of acetone and diesel are given in **Table 1.** Precision scale were used to prepare the mixtures. Mixtures were formed by adding 5% and 10% acetone to each 1000 g of diesel fuel. The mixture with 5% acetone was named A5D05, and the mixture with 10% acetone was named A10D90.

Table 1 Acetone and Diesel Specifications

Specifications	Acetone (C_3H_6O)	Diesel
Boiling point	56.2 °C (1013 hPa)	-
Density	0.79 g/cm3 (20 °C)	820-845 kg/cm3
Explosion limit	2.6 - 12.8 %(V)	-
Flash point	-17.0 °C	55 °C
Auto-ignition Temperature	465 °C DIN 51794	186–230 °C
Higher Heating Value(HHV)	-	45.6 MJ/kg
Low heat Value (LHV)	29.6 MJ/Kg	42.7 MJ/kg
Melting Point	-94.0 °C	-
pH value	5 - 6(395 g/l, H_2O, 20 °C)	-
Vapor pressure	24.53 kPa (20 °C)	< 1 kPa (38°C)
Cetane Number	-	51
Viscosity	-	2.0- 4.5 mm^2 /s

The experiment was carried out on the test engine in Erciyes University Engines Laboratory. The features and visual of the test engine are given in **Fig.1** and **Table 2**, respectively.

Fig. 1. Test Engine

Table 2 Engine Specifications

Test engine	NİSSAN PE6H
Bore	133 mm
Stroke.	140 mm
Number of cylinders	6
Displaced volume	11670 cc
Max. Power	234 Hp
Max. Speed	2300 rpm
Max. Torque	724 Nm (at 2300 rpm&234hp)
Compression ratio	16.5
Injection timing	16 'BTDC
Nozzle opening pressure	200 kg/cm^2 (2850 psi)
Firing order	1-4-2-6-3-5
Valve clearance (COLD)	In. 0.4 mm, Exh. 0.4 mm

2.3 Methods

The experiments were carried out at a constant engine speed of 600 rpm, under a load of 100, 200, 300 Nm, respectively, using pure diesel, A5D95 and A10D90 fuels, respectively. Theoretically, the maximum torque value was calculated as 724 Nm according to the maximum torque and power value on the label value of the test engine. Experimentally, a maximum torque of 350 Nm has been reached at 600 rpm. The percentage values of 3 different torque values used in the experiments according to the maximum torque value at 600 rpm correspond to 29, 57 and 86% for 100, 200 and 300 Nm, respectively. A total of 9 sets of experiments were conducted. Before starting the experiments, the fuel in the engine was completely drained and this process was repeated when each fuel type was changed. In the experiments, fuel consumption was determined by measuring with precision balance. Fuel consumption measurements were recorded in 5-minute periods. In-cylinder pressure values were recorded separately for each load and each fuel type, thanks to a piezoelectric sensor. Engine performance data such as engine speed, load and exhaust temperature were taken from the engine performance measurement program screen. Exhaust emission values were obtained with Bosch BEA 60 emission analyzer. Recordings were taken in each experimental set.

Experiments were first started with pure diesel. Then, it was continued with A5D95 and A10D90 fuel type, respectively. The recorded values for each set of experiments were analyzed and the results were presented in section 3.

3. RESULTS, FIGURES AND TABLES

3.1 Engine Performance

Brake thermal efficiency (BTE) is a function of the braking power produced by an internal combustion engine and the thermal energy of the fuel entering the engine.

Thus, it is calculated how much of the fuel energy entering the engine is converted into useful work.[7] In this study, BTE calculation was made using equation (1). In equation 1: Pb; Braking power, ṁf; fuel flow rate, LHV; the lower heating value of the fuel.

$$\eta_{th} = \frac{P_b}{\dot{m}f \text{ x LHV}} \tag{1}$$

The LHV values of the mixtures were calculated using Equation (2).

$$LHV_K = \frac{m_b x LHV_b + m_m x LHV_m}{m_b + m_m} \tag{2}$$

In equation 2: m_b; amount of first fuel, m_m; amount of second fuel, LHV_b; lower heat value of first fuel, LHV_m; the lower heat value of the second fuel.
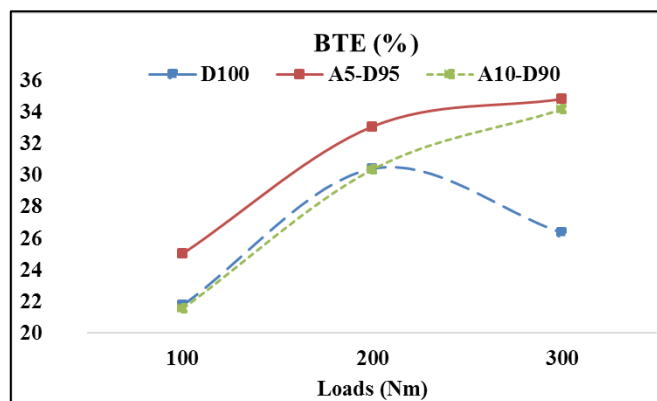
Fig. 2. Brake Thermal Efficiency (BTE)

Table 3 BTE values (%)

BTE	100 Nm	200 Nm	300 Nm
D100	21.77	30.43	26.37
A5-D95	25.04	33.10	34.85
A10-D90	21.54	30.38	34.20

The BTE values and graph obtained as a result of the experiments are shown in **Table 3** and **Fig.2**, respectively. A5D95 fuel has the highest BTE value at all loads. Although D100 and A10D90 had very close BTE values at 100 and 200 Nm loads, the BTE value of D100 fuel decreased sharply at 300 Nm load. Actually, this is not expected, it is thought that the reason for this may be measurement error.

Brake specific fuel consumption (BSFC) indicates how efficiently fuel is used in a power generating internal combustion engine [8]. It is the amount of fuel consumed per brake power produced. BSFC values were calculated using equation (3). In equation 3: Pb; Braking power, ṁf; represents the fuel flow rate.

$$bsfc = \frac{\dot{m}_f}{P_b} \quad (g / kW.h)$$

(3)
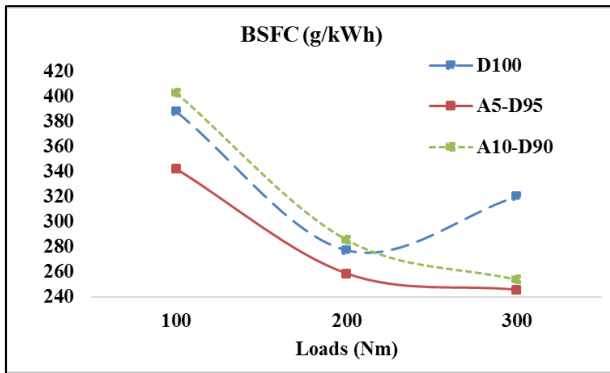
Fig. 3. Brake Specific Fuel Consumpsion (BSFC)

Table 4 BSFC values (g/kWh)

BSFC	100 Nm	200 Nm	300 Nm
D100	387,299	276,985	319,705
A5-D95	341,619	258,481	245,489
A10-D90	402,622	285,449	253,581

The BSFC value of the A5D95 fuel with the highest BTE value has the lowest value as expected. As with BTE values, BSFC values of D100 and A10D90 fuels were observed to be close under 100 and 200 Nm loads. D100 fuel has the highest BSFC value under 300 Nm load and therefore the lowest BTE value at 300 Nm load.

It is seen from the graphs and tables above that the BTE value of A5D95 fuel is 3.27, 2.67 and 8.48% higher than D100 fuel under 100, 200 and 300 Nm load, respectively. Likewise, A5D95 fuel is 3.5, 2.72 and 0.83% more efficient than A10D90 fuel.

In order to understand the reason for this, it would be useful to divide the graph of the in-cylinder pressure into phases as in **Fig. 4** and examine it. 1. Phase: After fuel is injected into the cylinder, the fuel does not ignite immediately, there is a delay period for the fuel to ignite. This process refers to the time from the moment of fuel injection to the start of combustion. The most important factor affecting the 1st phase is the ignition temperature of the fuel. The shorter the ignition delay, the better the combustion in the cylinder. 2. Phase: This phase starts at the moment of inconsistency of the in-cylinder pressure and lasts until the pressure spike. In this phase, with oxygen molecules that dissociate into atoms, hydrocarbons that dissociate into atoms form OH molecules and the combustion process begins. A significant amount of the heat generated at the beginning of combustion is used to evaporate the fuel injected into the cylinder. The decrease in in-cylinder pressure in this phase is due to the heat used to evaporate the fuel. Since evaporation takes place by taking heat, it uses some of the heat inside the cylinder and this causes a pressure drop. The evaporation property of the fuel is the most important factor affecting this phase. 3. Phase: It is the process in which all of the injected fuel participates in the combustion and an

explosion occurs in the cylinder center. It is the region with the highest pressure and heat release. 4. Phase: This phase is the main combustion process of the fuel and is the process by which the combustion is converted into work. At the end of the phase, the maximum combustion temperature is reached and the pressure drops rapidly. The 5th and 6th phases are the fast pressure drop phase and the slow pressure drop phase, respectively [9].
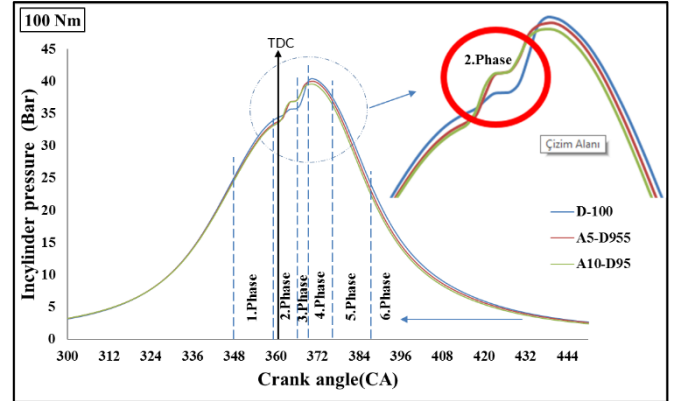
Fig. 4. Incylinder Pressure under 100 Nm load.
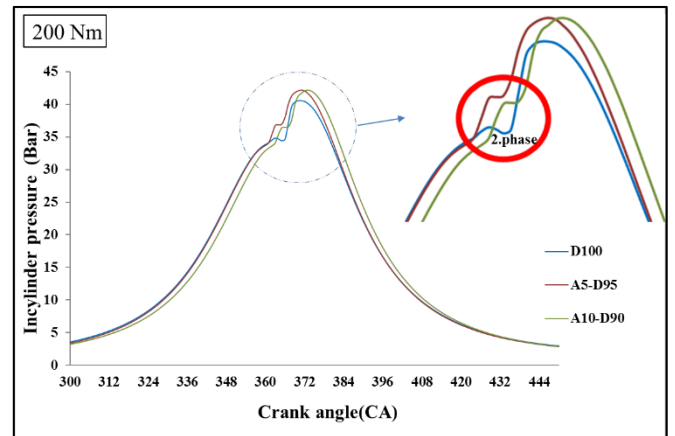
Fig. 5. Incylinder Pressure under 200 Nm load.
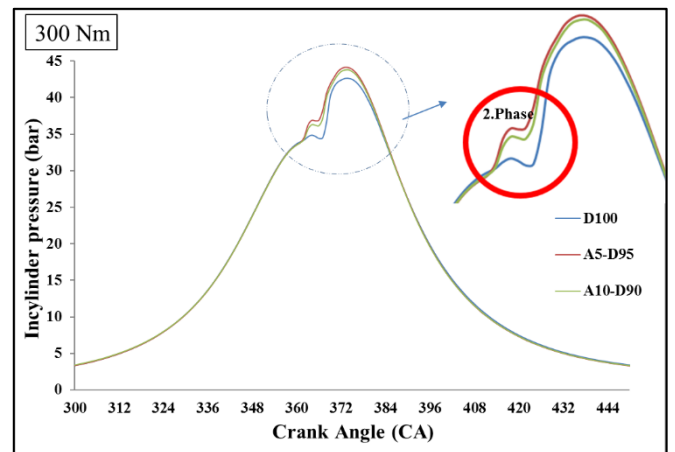
Fig. 6. Incylinder Pressure under 300 Nm load.

As seen in **Fig. 4, 5** and **6**, the highest pressure loss occurred in D100 (pure diesel) fuel in the 2nd phase region. Less pressure loss occurred in acetone-added fuels in the 2nd phase compared to D100 fuel. Acetone is more volatile than diesel because the vapor pressure of acetone (24.53 kPa (20 °C) [16]), is considerably higher than that of diesel (< 1 kPa (38°C) [17]). For this reason, fuels with

acetone additives used less of the heat generated at the start of combustion in the 2nd phase during evaporation compared to D100 fuel. Since there is less heat loss in the same phase, the pressure loss of acetone added fuels was less than D100 fuel. This resulted in an increase in efficiency in fuel with 5% acetone additive.

Contrary to volatility, since the auto-ignition temperature of acetone is higher than diesel fuel, 10% acetone additive increased the auto-ignition temperature of the mixture compared to pure diesel and caused relatively delayed combustion. This explains why the efficiency of 10% acetone additive fuel is low compared to D100 fuel. As a result, while acetone additive in low proportions (%5) increased the efficiency thanks to the high volatility of acetone, 10% acetone additive delayed the combustion and adversely affected the efficiency as it increased the auto-ignition temperature of the mixture.

3.2 Exhaust Emissions and Temperature

In **Fig. 7**, the CO emission amounts per power are given. While the lowest CO emission at 100 Nm load belongs to D100 fuel, at high loads (100, 200 Nm) the lowest CO emission belongs to A5D95 fuel. The CO emission of A10D90 fuel is higher than other fuel types at all loads. Since slow oxidation occurs with the decrease in in-cylinder pressure and temperature, CO emission occurs. Incomplete combustion and incomplete combustion time are another factor that increases CO emissions [10]. In this study, in-cylinder pressure loss of fuel with 5% acetone additive in the second phase, especially at high loads (200, 300 Nm), is less than other fuels thanks to the high volatility of acetone. Thus, both in-cylinder pressure and temperature were preserved. For this reason, a better combustion occurred and CO emission was observed at lower values compared to other fuels. Since the auto-ignition temperature of acetone in 10% acetone added fuel is higher than diesel, it increased the auto-ignition temperature of the mixture. For this reason, the oxidation time was shorter than other fuels and late combustion occurred. This situation caused an increase in CO emissions in A10D90 fuel.
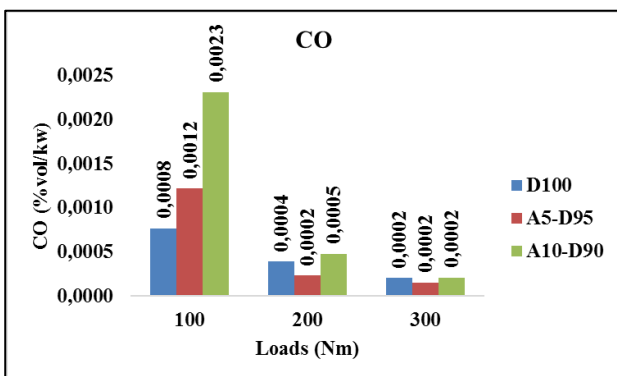
Fig. 7. CO Emission

Fig. 8 shows the CO_2 emission values. The lowest CO_2 emission at all loads belongs to A10D90 fuel. Especially at 100 and 200 Nm loads, the CO_2 emission rates of D100 and A5D95 fuels were observed to be very close to each other. Except for 300 Nm load, it is expected that CO_2 emissions will be low in A10D90 fuel, which has the

lowest thermal efficiency at other loads. Because the CO molecules are expelled from the exhaust without being oxidized to CO_2. In complete combustion, all hydrocarbons are expected to turn into CO_2 and H_2O. When there is no complete combustion, CO molecules cannot be oxidized to CO_2 and CO_2 emission is seen as low [10, 11]. In this study, since 10% acetone additive increased the auto-ignition temperature of the mixture to a higher value than D100 fuel, there was a late combustion and the CO molecules were ejected from the exhaust before they could be oxidized to CO_2. Therefore, its seen that the CO_2 rate is low compared to other fuel types in A10D90 fuel.
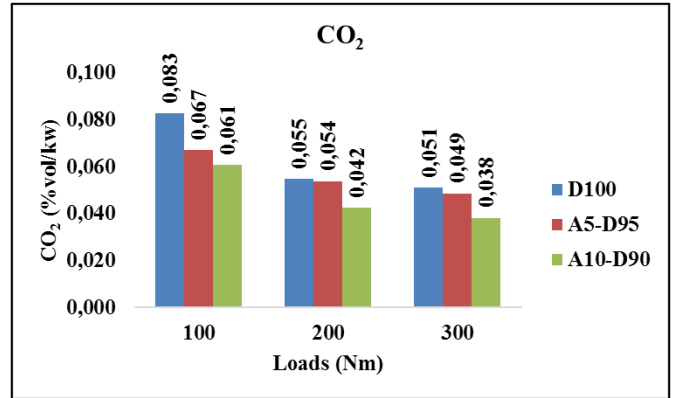
Fig. 8. CO_2 Emission

The combustion temperature in the cylinder and the length of the combustion period are the two most effective factors in the formation of NO_x emission [12-14]. Thanks to the high temperature, N_2 and O_2 molecules react by dissociating into their atons and NO_x emission occurs as a result of this reaction [13, 15]. NO_x emission values are given in **Fig.9**. In this study, the highest NO_x values occurred in A5D95 fuel. Although the exhaust temperature of the A10D90 fuel (**Fig. 10**) at 200 and 300 Nm loads was relatively higher than the A5D95 fuel, the amount of NO_x emission was quite low. The reason for this is delayed combustion due to the high spontaneous combustion temperature of the 10% acetone added fuel (A10D90) mixture and short burning time.
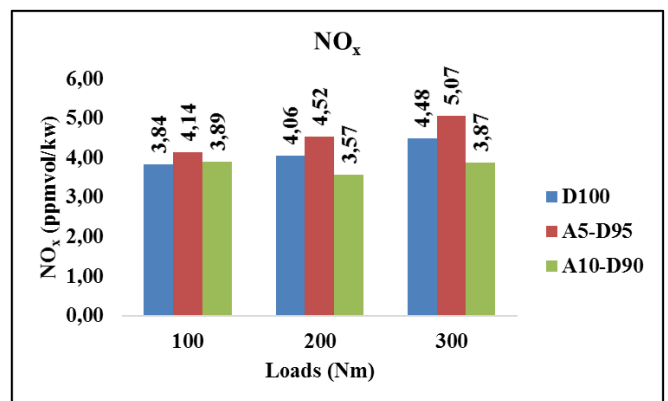
Fig. 9. NO_x Emission

It has been observed that the exhaust temperature of 5% acetone added (A5D95) fuel is higher than D100 (pure diesel) fuel. In other words, 5% acetone additive to pure diesel has an increasing effect on NO_x formation. Since there is the least heat and pressure loss in 5% acetone

added fuel (2nd phase, **Fig. 4, 5 and 6**), it has a longer burning time than D100 fuel. For this reason, although the exhaust temperature of A5D95 fuel is lower than that of D100 fuel, the amount of NO$_x$ has increased.
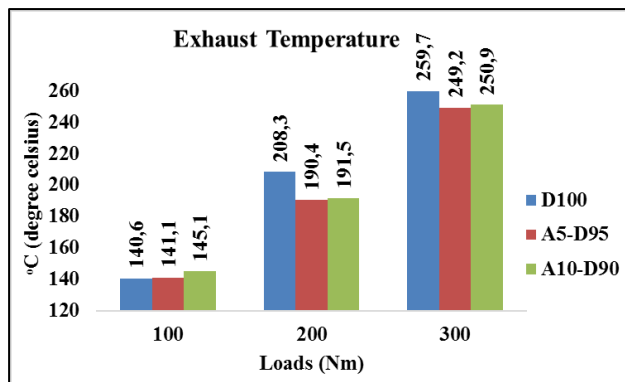
Fig. 10. Exhaust Temperature

4. CONCLUSION

Since the vapor pressure of acetone is higher than that of diesel, it is more volatile. Therefore, fuel with 5% acetone-added less heat and pressure loss at the beginning of combustion. In addition, the in-cylinder pressure graph of A5D95 fuel is better than other fuels. It has the highest pressure value especially at 200 and 300 Nm loads. For these reasons, it has been observed that the BTE value of 5% acetone added fuel is higher than other fuels. However, 10% acetone additive increased the auto-ignition temperature of the mixture due to the high auto-ignition temperature of acetone. Therefore, combustion was delayed compared to other fuels and efficiency loss occurred.

Since the efficiency of the fuel with 5% acetone additive is high, a better combustion has taken place compared to other fuels. This has contributed to the reduction of CO emissions. But it caused an increase in NO$_x$ emission. In summary, while the 5% acetone additive had a positive effect on the yield, the 10% acetone additive had a negative effect on the yield. While the 5% acetone additive improved the efficiency, it worsened the NO$_x$ emission, but improved the Co emission.

REFERENCES
[1]Turkey's Energy Outlook Report 2022 https://www.mmo.org.tr/merkez/basin-aciklamasi/enerji-gorunumu-raporu-ve-sunumu [accessed 12 December 2022]

[2] Yoon, S. H., Cha, J. P., & Lee, C. S. (2010). An investigation of the effects of spray angle and injection strategy on dimethyl ether (DME) combustion and exhaust emission characteristics in a common-rail diesel engine. Fuel Processing Technology, 91(11), 1364-1372.

https://doi.org/10.1016/j.fuproc.2010.04.017

[3] Keskin, A., Ocakoğlu, K., Reşitoğlu, İ.A.,(2013). Influence Of Titanium Based Fuel Additive On Diesel Engine Performance And Emissions. Journal of Gazi University Faculty of Engineering and Architecture, Vol. 28 ,No 3, 671-676,2013

[4] Sezer, İ. (2022), A rewiew study on the effects of dimethyl ether on engine preformance in diesel engines. Fuels, Fire and Combustion in Engineering Journal, Vol 10, No 1, 38-52,2022

[5] Aliustaoğlu, S., Ayhan, V.,(2019), The Effects Of Lpg-Diesel Dual Fuel Mixture On Performance And Smoke Emissions In A Direct Injection Diesel Engine. Journal of Advanced Technology Sciences, Volume 8, Issue 2, 109-116, 2019

[6] Ataman Chemicals Website:

https://www.atamanchemicals.com/acetone_u25157/?lang=TR [accessed 12 December 2022]

[7] Ramalingam, S., & Rajendran, S. (2019). Assessment of performance, combustion, and emission behavior of novel annona biodiesel-operated diesel engine. In Advances in eco-fuels for a sustainable environment (pp. 391-405). Woodhead Publishing.

https://doi.org/10.1016/B978-0-08-102728-8.00014-0.

[8] Ashok, B., & Nanthagopal, K. (2019). Eco friendly biofuels for CI engine applications. In Advances in Eco-fuels for a Sustainable Environment (pp. 407-440). Woodhead Publishing.

https://doi.org/10.1016/B978-0-08-102728-8.00015-2

[9] Olt, J., Mikita, V., Roots, J., & Jasinskas, A. (2015). Cylinder pressure characteristics of turbocharged and naturally aspirated diesel engines. Procedia Engineering, 100, 350-359.

https://doi.org/10.1016/j.proeng.2015.01.378

[10] Kül, V. S., & Akansu, S. O. (2022). Experimental Investigation of the impact of boron nanoparticles and CNG on performance and emissions of Heavy-Duty diesel engines. Fuel, 324, 124470.

https://doi.org/10.1016/j.fuel.2022.124470

[11] Paul, A., Panua, R. S., Debroy, D., & Bose, P. K. 2015. An experimental study of the performance, combustion and emission characteristics of a CI engine under dual fuel mode using CNG and oxygenated pilot fuel blends. Energy, 86, 560-573.

https://doi.org/10.1016/j.energy.2015.04.050

[12] Albayrak Ç. B, Yıldız M, Akansu S.O, Kahraman N. Performance and emission characteristics of an IC engine under SI, SI-CAI and CAI combustion modes, ENERGY, Vol. 136, p. 72-79, 2017

https://doi.org/10.1016/j.energy.2016.08.038

[13] YILDIZ, M., & ÇEPER, B. A. Experimental Study on an SI Engine Mapping Considering Performance, Emissions, and Cyclic Variability, Energy, Environment and Storage (2021) 01-01:42-49.

https://doi.org/10.52924/BBNP1133

[14] Liu, J., Yang, F., Wang, H., Ouyang, M., & Hao, S. (2013). Effects of pilot fuel quantity on the emissions characteristics of a CNG/diesel dual fuel engine with optimized pilot injection timing. Applied Energy, 110, 201-206.
https://doi.org/10.1016/j.apenergy.2013.03.024

[15] Pulkrabek, W W. Engineering Fundamentals of the Internal Combustion Engines, Novi Bios, 2021.

[16] Acetone CAS No. 67-64-1.
https://www.merckmillipore.com/TR/tr/product/Acetone, MDA_CHEM-100022 [accessed 23 December 2022]

[17] Opet MSDS form
 https://www.opet.com.tr/medium/document-file-21.vsf
[accessed 23 December 2022]
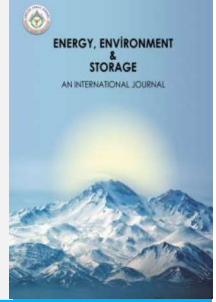
Numerical and Optimization Study on a Heat Exchanger Tube Inserted with Ring by Taguchi Approach

Toygun Dagdevir[1*],

[1]*Erciyes University, Dept. of Mechanical Engineering, Kayseri, Turkey, ORCID: 0000-0001-7388-3391*

ABSTRACT. This paper presents an optimizaton study on a heat exchanger tube inserted with circular rings by using numerical analysis results. Pitch length (50, 100 and 200 mm), inner diameter (15, 12.5 and 10.0 mm) and thickness (1, 3 and 5 mm) of the rings are considered as factors to be optimized. Water is selected as working fluid and the tube is considered under constant heat flux of 20 kW/m2 and turbulent flow condition. k-ε RNG turbulent model is used to simulate the turbulent flow thorugh the tube. L9 design of experiment model is used to reduce the number of numerical runs which is proposed by Taguchi method. The optimization study is conducted as single and multi objective optimization by using Taguchi method and Grey relation analysis. Furthermore, the contribution effects of the considered parameters on the Nusselt number and the friction factor result are revealed by ANOVA. Numerical resutls showed that the Nusselt number and the friction factor increases as the pitch length, the diameter and the thickness decreases. It is found that the most effective parameters on both the Nusselt number and the friction factor is inner diameter of the rings. For the single-objective optimization, the highest Nusselt number and the lowest friction factor is obtained with the tube configuration that are found as the pitch length of 50 mm, the diameter of 10 mm and the thickness of 5 mm and the pitch length of 200 mm, the diameter of 15 mm and the thickness of 3.0 mm, respectively. The pitch length of 50 mm, the diameter of 15.0 mm and the thickness of 5.0 mm presents the best thermal and hydraulic performance according to the multi-objective optimization study.

1. INTRODUCTION

Increasing in population, depleting the fossil fuel sources and improvements on technology cause to increase in energy demand and cost. Therefore, the efficient use of energy has become inevitable. Since heat energy is the most irreversible energy type, heat transfer enhancement studies are popular and necessary. Heat transfer enhancement techniques are classified in two groups such as active and passive[1]. Active techniques require extra power input to the system, while passive techniques are based on the physical modification on the system[2].The active techniques are not widely preferred due to having complexity, weight and control system, although they are successful in heat transfer. Therefore, the passive techniques are more preferred due to its advantageousness compared to the active techniques [3].

The most popular passive methods are coiled tubes [4], extended surfaces [5], rough surfaces [6], swirl flow devices (twisted tape) [7], conical ring [8], vortex rings [6] and coiled wire [9] etc. The common conclusion from the techniques applied for heat transfer enhancement increases not only Nusselt number (*Nu*), but also friction factor (*f*).

These two results are evaluated according to thermo-hydraulic performance criteria (THP) in literature. The THP value greater than 1.0 indicates that the applied technique is suitable for both thermal and hydraulic performance in practice.

Promvonge [10]investigated that the performance of conical rings for passive heat enhancement technique. They resulted that the enhancement in Nusselt number is achieved up to 197%, 333% and 237% for the use of CR, DR and CDR, respectively. They also reported correlations for the *Nu* and the *f* results belongs to conical ring used heat exchanger tube.

$$Nu = 0.09155 Re^{0.655} Pr^{0.4} \left(\frac{d}{D}\right)^{-1.31} \qquad (1)$$

$$f = 1.12 Re^{-0258} \left(\frac{d}{D}\right)^{-4.4} \qquad (2)$$

Promvonge and Eiamsa-ard [11] also investigated the effect of conical-nozzle turbulators on heat transfer and turbulent flow in a circular tube. Heat transfer, friction

*Corresponding author: toygun@erciyes.edu.tr

factor and thermo-hydraulic performance of a circular tube fitted with conical-ring and twisted tape inserts is experimentally investigated by Promvonge and Eiamsa-ard [12]. They found that the THP tends to decrease for using all conical-ring and twisted tape insert cases with the increment of Reynolds number. Kongkaitpaiboon et al. [13] investigated the perforated conical-ring on heat transfer enhancement. They found that the heat transfer rate and friction factor increase with decreasing number of perforated holes, pitch ratio. In addition to thermal and hydraulic performance researches, the cooling/heating systems need an optimum configuration including heat transfer enhancement technique. Majid et al. [14] conducted a research on optimization of heat transfer on helically coiled pipe flowing nanofluid using Taguchi method. Poornodoya et al. [15] optimized the performance parameters of a double pipe heat exchanger with cut twisted tape using respond surface method. Turgut et al. [16] researched the optimization of the concentric heat exchanger with injector turbulators by Taguchi method. Chamoli et al. [17] applied Taguchi method on flow and geometrical parameters in a rectangular channel roughened with down perforated baffles. Dagdevir [18] optimized the dimpled heat exchanger tube parameters according to multi-objective parameters such as the Nu and the f.

Since Taguchi method has a great advantageous with design of experiment which significantly reduce the number of the experimental or numerical runs [19], many researchers used the method to optimize their results.

According to the literature review, the passive heat transfer enhancement techniques promise to design better, lower size, energy saver heat exchangers, and Taguchi method is useful for optimizing the results and reduce the runs. It is recognized that there is a gap in the literature about optimization of circular tube fitted with circular ring on thermal and hydraulic performance. Therefore, it is focused on researching the thermal and hydraulic results and optimizing the parameters of a circular heat exchanger tube fitted with various rings arrays and dimensions in the present study.

2. MATERIALS ANDMETHODS

2.1 Numerical method

In order to investigate and optimize the circular tube inserted with rings, a solution domain is modeled as depicted in Fig. 1. The solution domain composes of three sections: entrance section, test section and exit section with lengths of 200 mm, 1000 mm and 100 mm, respectively. Inner diameter of the tube (D) is selected as 17.272 mm The results are considered for the test section; however, the entrance section and the exit section should be created for the insurances of the numerical procedure. On a hand, the test section is created to provide fully developed flow with a length at least ten times diameter of the tube, as suggested by Incropera et al. [20]. On the other hand, the exit section is created to prevent reverse flow error which is not nor mal to pressure outlet surface by rings.

In order to model a heat exchanger tube, a constant heat flux boundary condition is applied on the test section as 20 kW/m². Wall boundary conditions is assumed as no slip for entire sections. Inlet of the tube is assumed as velocity inlet and it is calculated according to Reynolds number. The outlet of the tube is selected as pressure outlet with gauge pressure of 0 Pa to simulate atmospheric condition.
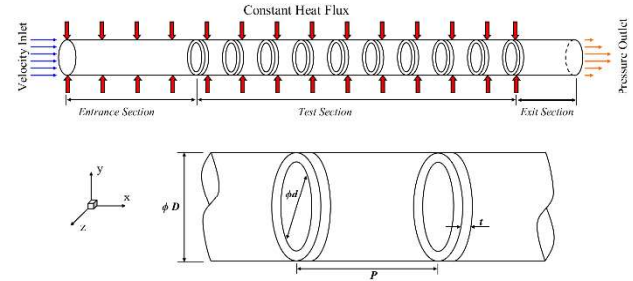
Fig. 1. Schematical view of the solution domain

2. 2 Governing equations

This study is conducted by employing the CFD software, Fluent version 18.0, which solves governing conservation equations with finite volume technique. The equations at steady state conditions are given as below [21]:

Mass conservation equation:

$$\nabla(\rho\vec{V}) = 0 \tag{3}$$

Momentum conservation equation:

$$\nabla(\rho\vec{V}\vec{V}) = -\nabla P + \nabla(\mu\nabla\vec{V}) \tag{4}$$

Energy conservation equation:

$$\nabla(\rho c_p\vec{V}T) = \nabla(k\nabla T) \tag{5}$$

where ρ is fluid density, V is velocity, P is pressure, μ is dynamic viscosity, cp is specific heat capacity, k is thermal conductivity, and T is temperature. RNG turbulence model is adopted for the all cases. The RNG transport equation for kinetic energy k and ε turbulence dissipation:

$$\frac{\partial}{\partial t}(\rho k) + \frac{\partial}{\partial x_i}(\rho k u_i) = \frac{\partial}{\partial x_j}(\alpha_k \mu_{eff} \frac{\partial k}{\partial x_j}) + G_k + G_b - \rho\epsilon - Y_m + S_k \tag{6}$$

$$\frac{\partial}{\partial t}(\rho\epsilon) + \frac{\partial}{\partial x_i}(\rho\epsilon u_i) = \frac{\partial}{\partial x_j}(\alpha_\epsilon \mu_{eff} \frac{\partial\epsilon}{\partial x_j}) + C_{1\epsilon}\frac{\epsilon}{k}(G_k + C_{3\epsilon}G_b) - C_{2\epsilon}\rho\frac{\epsilon^2}{k} - R_\epsilon + S_\epsilon \tag{7}$$

In these equations, G_k represents the generation of turbulence kinetic energy due to the mean velocity gradients. Gb is the generation of turbulence kinetic energy due to buoyancy. Y_m represents the contribution of the fluctuating dilatation in compressible turbulence to the overall dissipation rate. The quantities α_k and α_ε are the inverse effective Prandtl numbers for k and respectively. S_k and S_ε are user-defined source terms. Detail information is available in Fluent Theory Guide [21].

$$C_2^* = C_{2\epsilon} + \frac{C_\mu \eta^3 (1 - \eta/\eta_0)}{1 + \beta \eta^3} \quad (8)$$

$$\eta = Sk/\epsilon S = (2S_{ij}S_{ij})^{1/2} \quad (9)$$

Used constants of the turbulence model are given as below:

$$C_\mu = 0.0845, \quad \sigma_k = 0.7194, \sigma_\epsilon = 0.7194,$$

$$C_{\epsilon 1} = 1.42, \quad C_{\epsilon 2} = 1.68, \quad \eta_0 = 4.38, \quad \beta = 0.012 \quad (10)$$

Semi Implicit Method for Pressure Linked Equations (SIMPLE) algorithm scheme is conducted to achieve the relationship between pressure and velocity coupling to enforce mass conservation and to obtain pressure field [21]. Quadratic Upstream Interpolation for Convective Kinematics (QUICK) scheme is used for discretion of convection terms and diffusion terms. The residual criteria of continuity, velocities, energy, k and ε are taken as 1×10^{-5} to ensure convergence of the solution.

2.3 Data reduction
Used data are exported from the software with area-weighted average by using surface integral. The Reynolds number (Re), which is ratio of inertial force to viscous force, is expressed as:

$$Re = \frac{\rho D V}{\mu} \quad (11)$$

where ρ density of the fluid, D is diameter of the tube, V velocity of the fluid and μ is dynamic viscosity of the fluid.

The average Nusselt number ($\overline{Nu}$), which is ratio of convective heat transfer rate to conductive heat transfer rate, is expressed as:

$$\overline{Nu} = \frac{\overline{h} D}{k} \quad (12)$$

k is thermal conductivity of the fluid, and the average convective heat transfer coefficient ($\overline{h}$) along the test section is calculated as:

$$\overline{h} = \frac{q''}{\varDelta T} \quad (13)$$

q'' is constant heat flux applied onto the wall surface of the entrance and test section. The average temperature difference ($\varDelta T$) in this equation is expressed as:

$$\varDelta T = T_s - T_b \quad (14)$$

where T_s is wall surface of the test section temperature and T_b is the fluid bulk temperature between inlet and outlet of the test section.

The friction factor (f) is expressed as:

$$f = \frac{\varDelta P}{\frac{1}{2}\rho V^2 \frac{L_{test}}{D}} \quad (15)$$

where ΔP is the pressure difference between inlet and outlet along the test section. L is the length of the test section of the tube.

2.4. Optimization study
The adopted optimization method is used as a paper published by author [18]. Taguchi method is a well-known and beneficial optimization tool due to providing minimum number of experiments determining the best choices of factors affecting the output responses. Because Taguchi method presents only single-objective optimization, Grey relation analysis is applied for a multi-objective optimization. Furthermore, relative contribution effects of the optimized parameters on the output are investigated with using Analysis of variance (ANOVA). Followed steps of the present study are given as the flow chart in Figure 2.
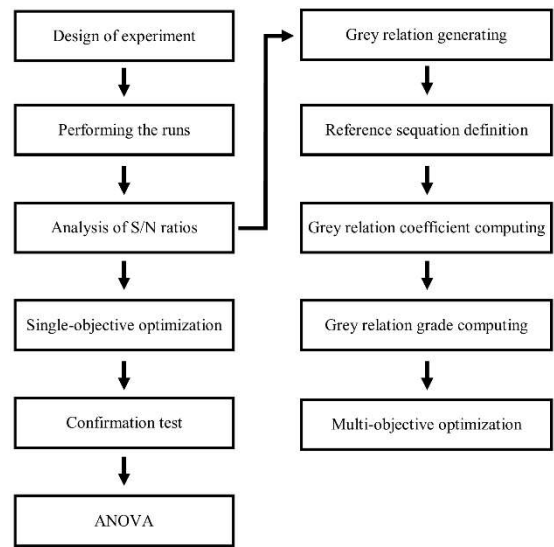
Fig 2. Flow chart of the followed step in the Taguchi method based Grey relation analysis

2.4.1. Design of experiments (DoE)
Taguchi method employs orthogonal arrays to ensure a broad performance of full-factorial experiment [22]. These orthogonal suggests a specific course of action of fragmentary analysis of the influencing parameters and their levels [17]. In this way, time and cost are significantly saved by reducing the number of experiments. The number of required experiment (Ln) is determined with Eq. (16) by the Taguchi method [23]. N_v and N_m represent the number of the variables and the number of maximum levels, respectively.

$$L_n = 1 + N_v[N_m - 1] \quad (16)$$

Table 1 Factors and levels used in the study

Factors	Levels

	1	2	3
Pitch length of rings (P) [mm]	50	100	200
Diameter of rings(d) [mm]	15.0	12.5	10.0
Thickness of rings (t) [mm]	1.0	3.0	5.0

These orthogonal arrays prescribe specific arrangement of fractional experiments with regard to the influencing factors and their levels. The present study adopts L9 orthogonal array including 3 factors with 3 levels given in Table 1. Thanks to the advantageous of the Taguchi method, the experiment number is reduced from 27 to 9. The design of experiments (DoE) according to L9 orthogonal array is given in Table 2.

Table 2 Plan for numerical runs

Runs no.	P	d	t
1	1	1	1
2	1	2	2
3	1	3	3
4	2	1	2
5	2	2	3
6	2	3	1
7	3	1	3
8	3	2	1
9	3	3	2

2.4.2. Signal to Noise ratio

The signal to noise ratios (SNR), denoting with η, of the experiments are obtained from the Taguchi method. The highest SNR value indicates the best level of the parameter. Since the purpose of the study is to determine the highest Nu and the lowest f, functions of "the larger is better" (Eq. (17)) and "the smaller is better" (Eq. (18)) are selected for the Nu and the f, respectively.

$$\eta = -10 log \left(\frac{1}{n} \sum_{i=1}^{n} \frac{1}{Y_i^2} \right) \tag{17}$$

$$\eta = -10 log \left(\frac{1}{n} \sum_{i=1}^{n} Y_i^2 \right) \tag{18}$$

2.4.3. ANOVA

Furthermore, analysis of variance (ANOVA) is carried out to evaluate the relative contribution effects of the parameters on the Nu and the f. ANOVA uses SNR data obtained from the Taguchi method. In this study, confidence level of the statistical analysis is selected as 95%. F-test is performed to ensure statistically reliability of the procedure. The relevant parameter is statistically significant, if the calculated F-test value is higher than F value. Used equations of the ANOVA are given in from Eq. (19) to Eq. (25).

$$SS_m = \frac{(\sum \eta_i)^2}{j} \tag{19}$$

$$SS_T = \sum \eta_i^2 - SS_m \tag{20}$$

$$SS_A = \frac{(\sum \eta_{Ai}^2)^2}{N} - SS_m \tag{21}$$

$$SS_E = SS_T - \sum SS_A \tag{22}$$

$$V_A = \frac{SS_A}{dof_A} \tag{23}$$

$$dof_A = n_A - 1 \tag{24}$$

$$F_{A0} = \frac{V_A}{V_E} \tag{25}$$

2.4.4. Grey relation analysis

Taguchi method is not sufficient to optimize more than one output, simultaneously, which can be called as multi-objective optimization. Grey relation analysis (GRA) is used to optimize multi-objective problems. In this study, the multi-objective problem is to find the configuration of the dimple parameters that give highest Nu and lowest f, simultaneously.

The GRA steps consist of main three steps:
1. Normalization of the experimental results
2. Calculation of grey relation coefficients (GRC) of the normalized data
3. Calculation of grey relation grades (GRG)

The normalization criteria as "*Higher is better*" (Eq. (26)) and "*Lower is better*" (Eq. (27)) are selected for the Nu and the f, respectively.

The higher is better:

$$x_i^*(k) = \frac{x_i^0(k) - min x_i^0(k)}{max x_i^0(k) - min x_i^0(k)} \tag{26}$$

$$x_i^*(k) = \frac{max x_i^0(k) - x_i^0(k)}{max x_i^0(k) - min x_i^0(k)} \tag{27}$$

Where $x_i^k(k)$ is the normalized value of the kth element in the ith sequence and $max x_i^0(k)$ and $min x_i^0(k)$ represent the highest and the lowest value of $x_i^k(k)$. After the normalization, the GRC (ξ_i) is calculated with the following Eqs. (28-31). Δ_{0i} given in Eq. (29) is the absolute value of the difference of the reference sequence ($x_0^*(k)$) and comparable sequence ($x_i^*(k)$). ζ is the distinguish coefficient ranging between 0 and 1, and it is generally used as 0.5 [24], [16], [25], [26], Δ_{min} and Δ_{max} are the lowest and the highest value of Δ_{0i}, respectively.

$$\xi_i(k) = \frac{\Delta_{min} + \zeta \Delta_{max}}{\Delta_{0i}(k) + \zeta \Delta_{max}} \tag{28}$$

$$\Delta_{0i} = \|x_o^*(k) - x_i^*(k)\| \tag{29}$$

$$\Delta_{min} = \frac{min}{\forall j \in i} \frac{min}{\forall k} \|x_o^*(k) - x_j^*(k)\| \tag{30}$$

$$\Delta_{max} = \frac{max}{\forall j \in i} \frac{max}{\forall k} \|x_o^*(k) - x_j^*(k)\| \tag{31}$$

Based on GRC, GRG (γ_i) representing the level of the correlation between the reference sequence and comparability sequence is calculated by Eq. (32).

$$\gamma_i = \frac{1}{n} \sum_{i=1}^{n} \xi_i(k) \tag{32}$$

3. RESULTS AND DISCUSSIONS

3.1. Validation of the numerical methodology

Comparisons of the results the present study both the smooth tube according to the Nusselt number and the

friction factor are given in Fig. 3. Gnielinski Eq. (33) [27] and Petukhov Eq. (34) [28] are used to compare with the results of the present study according to the Nusselt number and the friction factor, respectively. As can be seen from these figures that a good agreement is obtained between the present study and the literature.

$$Nu = \frac{(f/8)(Re_D - 1000)Pr}{1 + 12.7(f/8)^{1/2}(Pr^{2/3} - 1)} \quad (33)$$

$$f = (0.79ln(Re) - 1.64)^{-0.2} \quad (34)$$
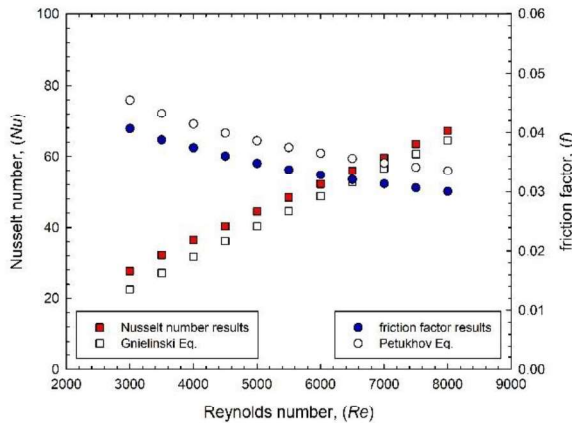
Fig 3. Comparison of results between equations in the literature

3.1. Heat Transfer

3.1.1. Effect of pitch length of the rings
Temperature contours for the cases having various pitch length by holding the inner diameter of 12.5 mm and the thickness of 3.0 mm constant are given in Fig. 4. As observed from the figure that the thermal boundary layer is destructed more significantly as the pitch length of the rings decreasing which led to increase heat transfer through the tube. On the other hand, the decrease in the pitch length of the rings means to the increment of the number of the rings through the test tube. Therefore, the increase in the number of the ring through the tube has a positive role on increase in heat transfer rate.
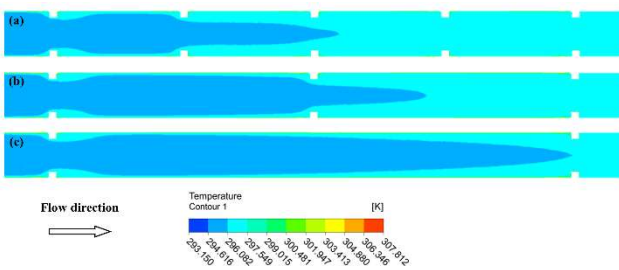

Fig 4. Temperature contours for various pitch length of the rings (a) P=50mm, b) P=100mm and c) P=200mm) by holding the inner diameter of 12.5 mm and the thickness of 3 mm.

3.1.2. Effect of inner diameter of the rings
Fig. 5shows the temperature contours of the cases having various inner diameter of the rings by holding the pitch length of 100 mm and the thickness of 3.0 mm constant.

The decrease in the inner diameter of the rings cause to more thermal boundary layer destruction by preventing the flow. The decrease in the inner diameter of the ring leads to compress the fluid in the core of the tube. As a result, the decrease in the inner diameter of the rings increase the heat transfer rate at behind of the rings.
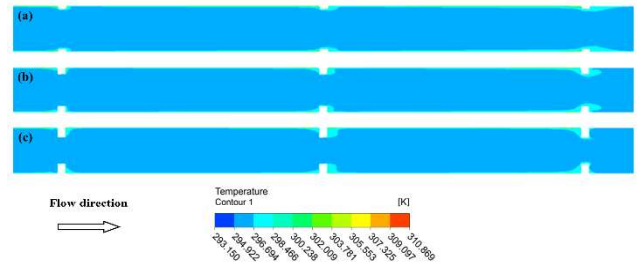

Fig 5. Temperature contours for various inner diameter of the rings (a) d=15.0 mm, b) d=12.5 mm and c) d=10.0 mm) by holding the pitch length of 100 mm and the thickness of 3 mm.
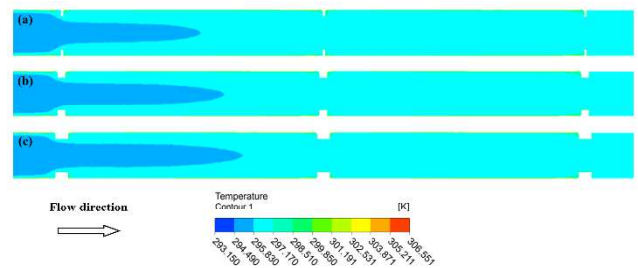
Fig 6. Temperature contours for various thickness of the rings (a) t=1mm, b) t=3mm and c) t=5mm) by holding the inner diameter of 12.5 mm and the pitch length of 100 mm.

3.1.3. Effect of thickness of the rings
Fig. 6 shows the temperature contours of the cases having various thickness of the rings by holding the pitch length of 100 mm and the inner diameter of 12.5 mm constant. The effect of the thickness of the rings for heat exchanger tube inserted with rings can be discussed by examining the figure. The region where there is no flow is much more heated by the heat flux, which lead to heat energy is stored. Furthermore, the length of the flow having low temperature increases with the increment of thickness of the rings. As a result, the thickness of the rings has a positive role on heat transfer enhancement.

3.2. Flow characteristic

3.2.1. Effect of pitch length of the rings
Velocity contours of the cases having various pitch lengths of the rings by holding the inner diameter of 12.5 mm and the thickness of 3 mm are given in Fig. 7. It is expected that the velocity of the fluid which flow in the ring increases due to decrease in cross sectional area of the path. This result is attributed to mass conversation. The rings at the inner wall surface of the tube creates more friction due to pressure drop. An increase the number of used rings through the tube increase the pressure drop directly. Therefore, the decrease in the pitch length increases the friction factor and pressure drop through the tube.
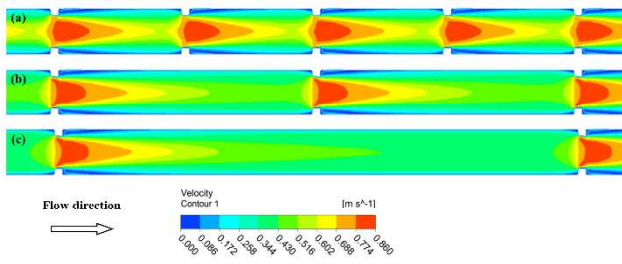
Fig 7. Velocity contours for various pitch length of the rings (a) P=50mm, b) P=100mm and c) P=200mm) by holding the inner diameter of 12.5 mm and the thickness of 3 mm.

3.2.2. Effect of inner diameter of the rings

The decrease in the inner diameter of the ring leads to compress the fluid in the core of the tube which cause to increase velocity. This result can be clearly from the Fig. 8. On the other hand, the decrease in the inner diameter of the ring increases the obstacle surface area through the flow path which cause to pressure drop penalty and so the friction factor.
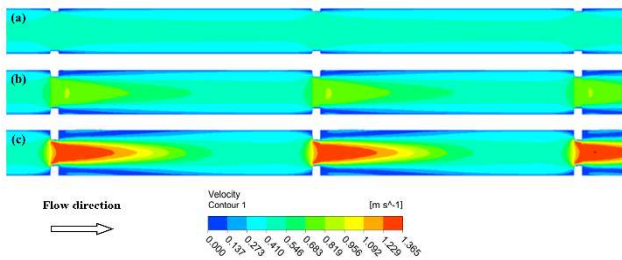
Fig 8. Velocity contours for various inner diameter of the rings (a) d=15.0 mm, b) d=12.5 mm and c) d=10.0 mm) by holding the pitch length of 100 mm and the thickness of 3 mm.

3.2.3. Effect of thickness of the rings

The velocity contour of various thickness of the rings is shown in Fig. 9. As the thickness of the ring increases, the wake region behind the ring increases. Besides, as the length of the flow path inside the ring becomes longer, the velocity magnitude at the regions, where the rings are placed, decreases compared to other counterparts. As a result, it can be stated that the increase in velocity magnitude through the tube cause to increase friction factor.
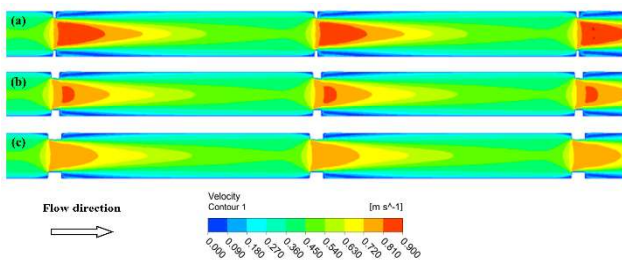

Fig 9. Velocity contours for various thickness of the rings (a) t=1mm, b) t=3mm and c) t=5mm) by holding the inner diameter of 12.5 mm and the pitch length of 100 mm.

3.3. Optimization

The effect of considered heat exchanger tube inserted with rings that are pitch length, inner diameter and thickness of the rings are discussed according to heat transfer and flow characteristic. An optimum configuration will be revealed at this section according to single and multi-objective optimization techniques.

Table 3 Results obtained by the numerical study and Taguchi method

Run	Factors			Results		SNR	
	P	d	t	Nu	f	Nu	f
1	1	1	1	108.18	0.1590	40.683	15.973
2	1	2	2	130.10	0.6849	42.286	3.288
3	1	3	3	171.03	2.6893	44.662	-8.593
4	2	1	2	95.10	0.0865	39.563	21.258
5	2	2	3	111.54	0.3506	40.949	9.104
6	2	3	1	144.89	1.9904	43.221	-5.979
7	3	1	3	87.81	0.0622	38.871	24.123
8	3	2	1	99.60	0.2679	39.965	11.442
9	3	3	2	115.10	0.7872	41.221	2.079

3.3.1. Single-objective optimization

Taguchi method is adopted to reveal an optimum configuration according to heat transfer and flow characteristic identically. The *Nu* and the *f* results are used to evaluate the heat transfer and the flow characteristic of the considered tube, respectively. The SNR (signal to noise ratio) values obtained from the Taguchi method according to the numerical results are given in Table 3.

The average SNR values for the *Nu* are given in Table 4 and plotted in Fig. 10. The optimum configuration is A1B3C3 corresponding to the pitch length of 50 mm, inner diameter of 10.0 mm and thickness of 5 mm according to the *Nu*.

Table 4 Average SNR values for the *Nu*

Factors	Levels		
	1	2	3
A: Pitch length (P)	42.54*	41.24	40.02
B: Inner diameter (d)	39.71	41.07	43.03*
C: Thickness (t)	41.29	41.02	41.49*
Mean 41.04 dB.			
* Optimum level			

The average SNR values for the *f* are given in Table 5 and plotted in Fig. 11. The optimum configuration is A3B1C2 corresponding to the pitch length of 200 mm, inner diameter of 15.0 mm and thickness of 3 mm according to the *f*. This result also can be clearly seen from Fig. 11.
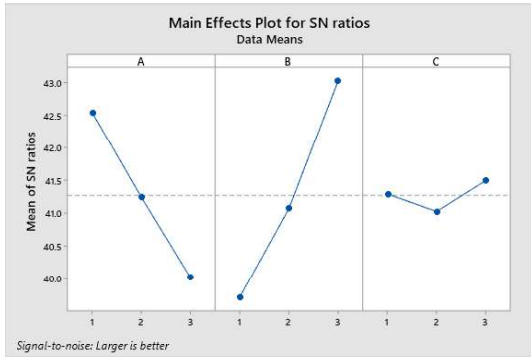
Fig 10. Mean effects plot for SNR for the *Nu*

Table 5 Average SNR values for the *f*

Factors	Levels		
	1	2	3
A: Pitch length (P)	3.556	8.128	12.548*
B: Inner diameter (d)	20.452*	7.945	-4.164
C: Thickness (t)	7.146	8.875*	8.211
Mean 8.077 dB.			
* Optimum level			
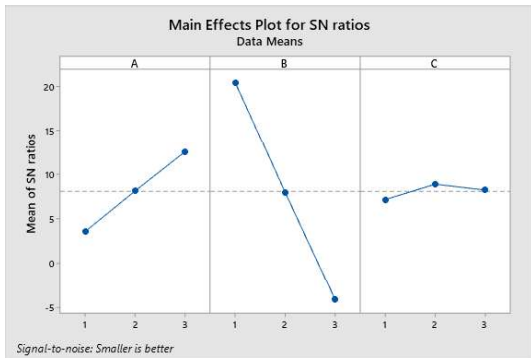
Fig 11. Mean effects plot for SNR for the *f*

3.3.2. ANOVA

Analysis of variance (ANOVA) study is performed on the SNR results from the Taguchi method to reveal the contribution effect of the factors on the Nu and the f. F-test with confidence level of 95% is used to assess the significance of the considered dimple parameters on the *Nu* and the *f*. Table 6 and Table 7 show the ANOVA results for the *Nu* and the *f*, respectively. F_{test} value being higher than $F_{0.05}$ indicates that the optimization study is confidence in %95 interval. Thereby, the confidence of the optimization study is ensured in %95 for the factors and for both the Nu and the *f*. According to Table 6 and Table 7, the most effective factor is inner diameter for both the Nu and the f, with of 61.88% and 87.38%, respectively. Besides, the confidence of the ANOVA is ensured by comparing the F-test value with $F_{0.05}$ values for both the *Nu* and the *f*.

Table 6 Average SNR values for the *Nu*

Factors	dof	SS	V	F-test	F_0.05	Cont. level (%)
P	2	9.5593	4.779	20.74	0.046	35.20
d	2	16.805	8.402	36.46	0.027	61.88
t	2	0.3336	0.166	0.72	0.580	1.23
Error	2	0.4609	0.230			1.70
Total	8					100

Table 7 Average SNR values for the *f*

Factors	dof	SS	V	F-test	F_0.05	Cont. level (%)
P	2	121.29	60.644	22.18	0.043	11.66
d	2	908.99	454.49	166.21	0.006	87.38
t	2	4.57	2.283	0.84	0.545	0.44
Error	2	5.47	2.734			0.53
Total	8	1040.32				100

3.3.3. Confirmation test

A confirmation test is performed to check whether the accuracy of the optimization methodology is accurate, or not. Initial parameters indicating the largest SNR value for both *Nu* and *f* are firstly selected to show the improvement in the SNR.A1B3C3 and A3B1C3are selected as the initial parameters for the *Nu* and the *f,* respectively. Then, the optimum parameters are predicted for both h and ΔP by using Eq. (17).

$$\hat{\eta} = \eta_m + \sum_{i=1}^{p}(\hat{\eta}_i - \eta_m) \qquad (35)$$

Where, $\hat{\eta}$ is the average of the SNR on the optimum level, η_m is the total average of the SNR and p is the number of parameters affecting the performance. According to confirmation test, it is found that the optimum configuration is also in the DoE. Since the predicted values for the *Nu* and the *f* would be same with the optimum values, the optimization methodology is ensured by confirmation test.

3.3.4. Multi-objective optimization

In order to reveal an optimum configuration indicating both the highest Nu and the lowest f, a multi-objective optimization study is performed by using Grey relation analysis (GRA). The obtained results of the GRA for the experiment plan are given in Table 8. According to the Table 8, 4th run(A2B1C2) present the optimum result which is the highest *Nu* and the lowest *f* in the DoE. The general optimum configuration can be apart from the experiment plan. For this scope, the Grey relation grade is generally calculated as plotted in Fig. 12. As read from this figure, the configuration providing the multi-objective optimization is A1B1C3 corresponding to the pitch length of 50 mm, the inner diameter of 15.0 mm and the thickness of 5.0 mm.

Table 8 GRA results for the numerical runs

Runs	Normalized data		Deviation sequence		Grey relation coefficient		Grey relation grade	Order
	Nu	f	Nu	f	Nu	f		
1	0.245	0.963	0.755	0.037	0.398	0.931	0.665	4
2	0.508	0.763	0.492	0.237	0.504	0.678	0.591	7
3	1.000	0.000	0.000	1.000	1.000	0.333	0.667	2
4	0.088	0.991	0.912	0.009	0.354	0.982	0.668	1
5	0.285	0.890	0.715	0.110	0.412	0.820	0.616	6
6	0.686	0.266	0.314	0.734	0.614	0.405	0.510	9
7	0.000	1.000	1.000	0.000	0.333	1.000	0.667	2
8	0.142	0.922	0.858	0.078	0.368	0.865	0.616	5
9	0.328	0.724	0.672	0.276	0.427	0.644	0.535	8
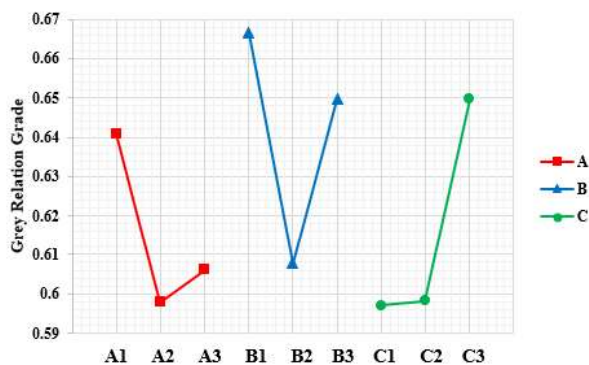
Fig 12. Effects of the parameters on multi-objective optimization

4. CONCLUSSION

The geometric parameters of a heat exchanger tube inserted with circular rings are numerically investigated and optimized according to the thermal and the hydraulic performance. In order to reduce the number of numerical runs design of experiment (DoE) by Taguchi method is used. The single-objective optimization which finds an optimum configuration is performed by Taguchi method according to the *Nu* or the *f*, while multi-objective optimization is performed by GRA according to both the *Nu* and the *f*. Besides, ANOVA is conducted to reveal the contribution effects of the factors on the *Nu* and the *f* results. The conclusions found from the studies are drawn in the following:

➢ The *Nu* and the *f* increases as the pitch length, the inner diameter and thickness of rings decreases.

➢ For the single-objective optimization, the highest *Nu* and the lowest *f* is obtained with the tube configuration that are A1B3C3 (i.e. the P of 50 mm, the d of 10 mm and the t of 5 mm) and A3B1C2 (i.e. the P of 200 mm, the d of 15 mm and the t of 3.0 mm), respectively.

➢ The contribution levels of the parameters are of P, d and t are determined for the *Nu* and the *f* as 35.20%, 61.88% and 1.23% and 11.66%, 87.38% and 0.44%, respectively.

➢ A1B1C3 (i.e. the P of 50 mm, the d of 15.0 mm and the t of 5.0 mm) presents the best thermal and hydraulic performance according to the multi-objective optimization study.

REFERENCES

[1]   M. Omidi, M. Farhadi, and M. Jafari, "A comprehensive review on double pipe heat exchangers," *Appl. Therm. Eng.*, vol. 110, pp. 1075–1090, Jan. 2017.

[2]   T. Alam and M.-H. Kim, "A comprehensive review on single phase heat transfer enhancement techniques in heat exchanger applications," *Renew. Sustain. Energy Rev.*, vol. 81, pp. 813–839, Jan. 2018.

[3]   L. Léal *et al.*, "An overview of heat transfer enhancement methods and new perspectives: Focus on active methods using electroactive materials," *Int. J. Heat Mass Transf.*, vol. 61, pp. 505–524, Jun. 2013.

[4]   D. Panahi and K. Zamzamian, "Heat transfer enhancement of shell-and-coiled tube heat exchanger utilizing helical wire turbulator," *Appl. Therm. Eng.*, vol. 115, pp. 607–615, 2017.

[5]   R. K. Shah, "Extended surface heat transfer," in *A-to-Z Guide to Thermodynamics, Heat and Mass Transfer, and Fluids Engineering*, Begellhouse.

[6]   M. Sheikholeslami, M. Gorji-Bandpy, and D. D. Ganji, "Review of heat transfer enhancement methods: Focus on passive methods using swirl flow devices," *Renew. Sustain. Energy Rev.*, vol. 49, pp. 444–469, Sep. 2015.

[7]   M. Uyanik, T. Dagdevir, and V. Ozceyhan, "Thermo-hydraulic performance investigation of a heat exchanger tube inserted with twisted tapes modified with various twist ratio and alternate axis," *Eur. Mech. Sci.*, vol. 6, no. 3, pp. 189–195, Sep. 2022.

[8]   M. M. Ibrahim, M. A. Essa, and N. H. Mostafa, "A computational study of heat transfer analysis for a circular tube with conical ring turbulators," *Int. J. Therm. Sci.*, vol. 137, pp. 138–160, Mar. 2019.

[9]   P. Promvonge, "Thermal performance in circular tube fitted with coiled square wires," *Energy Convers. Manag.*, vol. 49, no. 5, pp. 980–987, May 2008.

[10]   P. Promvonge, "Heat transfer behaviors in round tube with conical ring inserts," *Energy Convers. Manag.*, vol. 49, no. 1, pp. 8–15, Jan. 2008.

[11]   P. Promvonge and S. Eiamsa-ard, "Heat transfer and turbulent flow friction in a circular tube fitted with conical-nozzle turbulators," *Int. Commun. Heat Mass Transf.*, vol. 34, no. 1, pp. 72–82, Jan. 2007.

[12] P. Promvonge and S. Eiamsa-ard, "Heat transfer behaviors in a tube with combined conical-ring and twisted-tape insert," *Int. Commun. Heat Mass Transf.*, vol. 34, no. 7, pp. 849–859, Aug. 2007.

[13] V. Kongkaitpaiboon, K. Nanan, and S. Eiamsa-ard, "Experimental investigation of convective heat transfer and pressure loss in a round tube fitted with circular-ring turbulators," *Int. Commun. Heat Mass Transf.*, vol. 37, no. 5, pp. 568–574, May 2010.

[14]   M. Mohammadi, A. Abadeh, R. Nemati-Farouji, and M. Passandideh-Fard, "An optimization of heat transfer of nanofluid flow in a helically coiled pipe using Taguchi method," *J. Therm. Anal. Calorim.*, vol. 138, no. 2, pp. 1779–1792, Oct. 2019.

[15]   P. V. K. V. Kola, S. K. Pisipaty, S. S. Mendu,

and R. Ghosh, "Optimization of performance parameters of a double pipe heat exchanger with cut twisted tapes using CFD and RSM," *Chem. Eng. Process. - Process Intensif.*, vol. 163, p. 108362, Jun. 2021.

[16]   E. Turgut, G. Çakmak, and C. Yıldız, "Optimization of the concentric heat exchanger with injector turbulators by Taguchi method," *Energy Convers. Manag.*, vol. 53, no. 1, pp. 268–275, Jan. 2012.

[17]   S. Chamoli, P. Yu, and A. Kumar, "Multi-response optimization of geometric and flow parameters in a heat exchanger tube with perforated disk inserts by Taguchi grey relational analysis," *Appl. Therm. Eng.*, vol. 103, pp. 1339–1350, Jun. 2016.

[18]   T. Dagdevir, "Multi-objective optimization of geometrical parameters of dimples on a dimpled heat exchanger tube by Taguchi based Grey relation analysis and response surface method," *Int. J. Therm. Sci.*, vol. 173, p. 107365, Mar. 2022.

[19]   E. Dagdevir and M. Tokmakci, "Optimization of preprocessing stage in EEG based BCI systems in terms of accuracy and timing cost," *Biomed. Signal Process. Control*, vol. 67, p. 102548, May 2021.

[20]   T. L. Bergman, A. S. L. and F. P. Incropera, D. P. DeWitt, and A. S. Incropera, F. P., DeWitt, D. P., Bergman, T. L., & Lavine, *Fundamentals of heat and mass transfer*, 6th ed. New York: Wiley, 1996.

[21]   Fluent, "ANSYS Fluent User Guide." New Hampshire, 2016.

[22]   G. Taguchi, *Taguchi Techniques for Quality Engineering*. New York, 1987.

[23]   I. Kotcioglu, A. Cansiz, and M. Nasiri Khalaji, "Experimental investigation for optimization of design parameters in a rectangular duct with plate-fins heat exchanger by Taguchi method," *Appl. Therm. Eng.*, vol. 50, no. 1, pp. 604–613, Jan. 2013.

[24]   N. H. Naqiuddin *et al.*, "Numerical investigation for optimizing segmented micro-channel heat sink by Taguchi-Grey method," *Appl. Energy*, vol. 222, pp. 437–450, Jul. 2018.

[25]   S. Kumar and R. Singh, "Optimization of process parameters of metal inert gas welding with preheating on AISI 1018 mild steel using grey based Taguchi method," *Measurement*, vol. 148, p. 106924, Dec. 2019.

[26]   T. Dagdevir and V. Ozceyhan, "Optimization of process parameters in terms of stabilization and thermal conductivity on water based TiO2 nanofluid preparation by using Taguchi method and Grey relation analysis," *Int. Commun. Heat Mass Transf.*, p. 105047, Nov. 2020.

[27]   Gnielinski V., "New equations for heat and mass transfer in turbulent pipe and channel flow," *Int. Chem. Eng.*, vol. 27, pp. 359–368, 1976.

[28]   B. S. Petukhov, T. F. Irvine, and J. P. Hartnett, "Advances in heat transfer," *Acad. New York*, vol. 6, pp. 503–564, 1970.
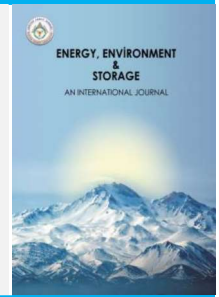
Assessment of CO and NO₂ pollutants concentration in the parking area and its relation to the occupancy percentage in the city of Makassar, Indonesia

Sattar Yunus[1*], Anugrah Yasin [2]

[1]*Department of Environmental Engineering, Universitas Muslim Indonesia, Makassar-90231, Indonesia*

[2] *Department of Civil Engineering, Universitas Fajar, Makassar-90231, Indonesia*

ABSTRACT. One of the sources of air pollution is exhaust emissions from vehicles during transportation activities. Due to the lack of parking spaces and the increase of the vehicles, many people park on the main roads, causing congestion on the side of the main roads. .When the engine is running and the vehicle is on stationed the engine's power is not used to turn the wheels, the combustion quality of the vehicle's engine is not so perfect and the exhaust gas is concentrated on a part of the road. To do, affects the ambient air quality of the location. The purpose of this study was to measure CO and NO₂ concentrations using the Impinger Air Sampler. Measurements were taken on the road bodies used for vehicle parking at four locations in Makassar city: Sombaopu street, Nusantara street, Mesjid Raya street and Jenderal Sudirman street. The data analysis used is a simple linear regression statistic to calculate occupancy. The analytical result obtained for the effect on occupancy and CO concentration was R^2= 0.51/51%, p<0.001, we can conclude that the effect of occupancy on CO concentration is significant. We can then conclude that at a value of R^2=0.64, p<0.001, the contribution of occupancy to changes in NO₂ concentration is also significant. we conclude that the contribution of this predictive model is 68%. Occupancy has a significant impact on CO and NO₂ concentrations in curbside parking areas.

Keywords: On the Street Parking, Vehicles, Air Pollution, Occupancy, Makassar City

1. INTRODUCTION

Today's transport sector is developing so fast that with an increasing number of city dwellers needing transport. The transport in the form of motorized traffic is being plagued by congestion, accidents, air pollution, noise pollution and land transport. It may lead to other effects caused road damage [1,2]. Stopping and starting motorized vehicles on city roads has a very large impact on hydrocarbon gas and carbon monoxide emissions [3,4]. Air pollution in many large cities is generally associated with the development of activities in the transport and industrial sectors, although the commercial and residential sectors still make important contributions [5]. One of them is caused by engine car exhaust gases that pollute the air, especially his Pb pollutants, CO, and dust in the form of coarse and fine particles [6,7].

The rapid growth of urbanization and industry in the Makassar city area as the largest city in Eastern Indonesia is inevitable, so that Makassar becomes a mixed commercial-residential-industrial area accompanied by an increase in the transportation sector which will cause air pollution problems including dust particles and also Carbon Black [8,9].

In line with that it was stated that air pollution due to transportation is mainly centered around urban areas and is principally caused by traffic in urban areas [10]. Improved transportation systems can also increase CO₂ and other greenhouse gas (GHG) emissions as well as VOCs [11]. The most significant increases in energy use and GHG emissions occur in metropolitan cities which have a rapid rate of population growth with a higher standard of living and level of affluence compared to rural areas or smaller cities [12]. These conditions distinguish one city from another metropolitan city. Several things that affect air quality are population, traffic density and fuel consumption as well as the area of green open space [13]. Because the tendency of air pollution is worrying from year to year, it is very important to carry out prevention and control efforts. Air pollution from transportation sources is to try to reduce pollution emissions from the source. Reducing pollution emissions at the source through technological improvements regarding environmental problems such as the development of electric propulsion systems, the use of

*Corresponding author: sattar.teknik@umi.ac.id

vegetable oil fuels or the use of environmentally friendly alternative fuels and so on, besides that it can also be done by developing [14].

Another effort that can be done is to develop an urban mass rapid transit system.

Several studies have also reported that an effective method for reducing pollution is to control the quantity (g) of air pollutants produced. Government legislation has been a driving force in reducing the amount of emissions of these pollutants with bans on coal and smoking, introduction of congestion charges and improving public transport to reduce the number of private vehicles on the roads [15,16]. It has been reported that a study on congestion in London in 2003 required significant resources in terms of implementation, infrastructure and policy enforcement and achieved a reduction of only 5-10% in the concentration of air pollution in the city [17]. Each control mechanism provides its own benefits with respect to improving air quality in urban environments. Implementing new government policies and laws is the basis for the continued success of current and proposed air pollution control strategies [18,19].

This study presents the concentrations of carbon monoxide and sodium hydroxide in the ambient air of a parking lot on four major streets of Makassar city: Somba Opu Street, Nusantara Street, Mesjid Raya Street and Jenderal Sudirman Street. Research on the relationship between air pollution and urban transport sector in Makassar city is still very limited. This study was conducted to find the level of air quality on highways used as parking lots and to solve some of the problems that arise when parking on the street due to parking difficulties. increase. The results are intended to inform the implementation of new policies by the city of Makassar and stakeholders, banning vehicles from stopping or even parking on certain roads, which are believed to cause congestion and worsening air quality. It is intended to enforce new regulations in place.

2. MATERIAL AND METHOD

2.1 Study Area
This research is about parking along the street body in the Makassar City area which causes congestion and air pollution in relation to environmental health. The location selection for the road is the parking area point in Makassar City which is determined purposively. The locations of this study are on the road in the center of Makassar, namely Somba Opu Street, Nusantara Street, Masjid Raya Street and Jenderal Sudiman Street as shown in **Figure 1.**

Considerations when deciding on street parking for motorized vehicles in Makassar city center include:

1. Observation deck on a log road with heavy traffic and many parking lots.

2. Observation sites are also centers of public activity such as commerce, catering and public utilities.

3. Areas of interest for trade and service zoning have been declared in sub-areas within the city of Makassar.
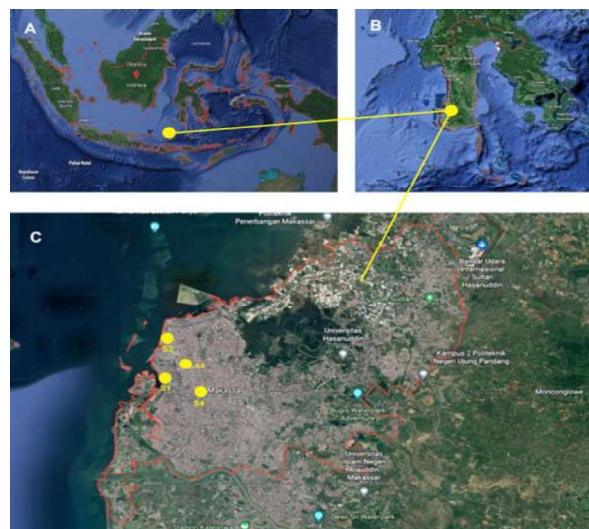

Fig. 1. Location of sampling sites in Makassar City; A.Map of Indonesia, B. Map of South Sulawesi Province, C.Map of Makassar City.

2.2 Data Collection
This research was conducted to measure the concentrations of CO and NO2 by using an Impinger Air Sampler (Model: MD-51MP). Impinger is an air sampling tool for ambient air. The accuracy of the analysis results is sufficient and this sampling method can be combined with measurement methods in the laboratory. Based on the principle of the chemical reaction of the capture solution with pollutant gas, an analysis is carried out on the results of the reactions that occur. In this method a certain amount of air is pulled by the impinger through a certain stable flow path. The adsorbent liquid reacts with the captured gas components and forms a specific and stable substance. The success of the impinger sampling method is influenced by several factors, including the perfection of gas absorption by the capturing solution, the accuracy of measuring air volume which is affected by pump stability, laboratory analysis and calculation and maintenance of equipment. Impinger equipment as a whole consists of:

- Vacuum pump: serves to draw air samples into the impinger.
- Impinger tube: where the reaction between airborne contaminants and the catcher solution
- Moisture adsorber: a tube containing a desiccant for protection
- pump from corrosion.
- Flow meter which measures the speed of air flow.

The standards used in sampling and analysis, namely for measuring the concentration of Carbon Monoxide, refer to the guidelines for measuring the Non-Dispersive Infra Red (NDIR) method listed on the Indonesian National Standard (SNI 7119.10.2005), while for measuring the concentration of Sodium Dioxide, it refers to measurement guidelines with the Griess_Salzman Method listed on the Indonesian National Standard (SNI 7119.2.2017).

3.3 Data Analysis

The data analysis used is descriptive analysis, namely by providing a description of the field data descriptively by interpreting the primary data into tabulations. This descriptive analysis aims to obtain an overview of the conditions and characteristics of the variables studied in each selected street parking lot (4 roads). Then analyzed with Occupancy analysis which includes calculation of travel time data, vehicle speed, vehicle dimensions, number of vehicles, occupancy time and parking area. Furthermore, Occupancy percentage is used to compare the four street parking locations that are used as data collection sites. Occupancy analysis results are associated with CO and NO_2 concentrations.

3. RESULTS AND DISCUSSION

In this section, the researcher describes the occupancy percentage rate at each observation location and its impact on environmental quality. The thing that needs to be understood again is that roadside parking barriers cause an increase in the time and percent occupancy of vehicles when crossing the road. Occupancy of vehicles on this road is the result of roadside obstacles that occur. The following graph illustrates the relationship between percent occupancy and environmental quality:

### 3.1. Comparison of Occupancy Percentage and Carbon Monoxide.
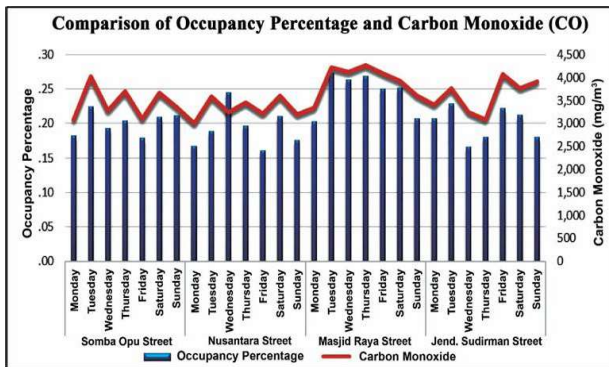
Fig 2. Comparison of occupancy percentage and CO

Figure 2 shows a comparison of utilization and CO. It can also be seen that, in general, the trend of day-to-day occupancy changes also follows changes in CO. Occupancy did not match changes in CO. However, Masjid Raya Street peak occupancy points also show the CO peak points for the four observed weeks. Occupancy Percentage and Nitrogen Dioxide (NO_2)

### 3.2. Comparison of Occupancy Percentage and Nitrogen Dioxide.
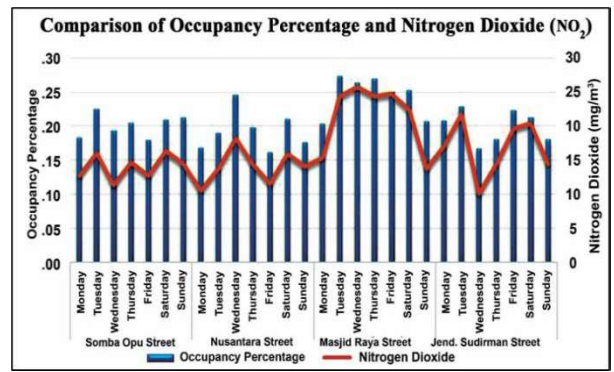
Fig 2. Occupancy Percentage and NO2

In Figure 2, it can be seen that the trend of occupancy percentage and NO_2 also shows indications of the same direction. At many observation points, an increase in percent occupancy also indicates an increase in NO_2. For example, on Jalan Masjid Raya on Tuesday, Wednesday and Thursday there was an increase in occupancy percentage which also showed a sharp increase in NO_2. The peak occupancy point on Jalan Masjid Raya is also the peak point for NO_2 during the observation.

3.3. Statistical Test of the Effect of Percent Occupancy on Air Quality with a Simple Linear Regression Test

The results of previous research have shown that there is a tendency that the occupancy dynamics on each street and every day of observation move in the same direction as the dynamics of air quality. In order to be able to detect the impact of percent occupancy on changes in pollutants that occurs, the researchers tested it statistically using a simple linear regression technique. The following are the results of testing the effect of percent occupancy of roads on environmental quality:

3.3.1. Occupancy Percentage Impact towards CO

Table 1. Regression Analysis of Occupancy Percentage Impact towards CO

Predictor	β	t	R	R^2	Adj. R^2	F
Persen Occupancy	0.713***	10.321	0.713	0.508***	0.504	106.5

Note: Dependent Variable : CO, N= 105; ***$p< .001$, **$p< .01$ and *$p< .05$

The results of observations on the impact of percent occupancy on CO showed a significant impact ($R2 = 0.51/$ 51%, $p < 0.001$). Similar to the previous analysis, this also shows the strong influence of percent occupancy on CO in the road. Furthermore, the analysis results also show that $\beta = 0.71$ ($p < 0.001$), which means that a 1% increase in percent occupancy results in an increase in CO up to 0.71 standard deviation. In general, it can also be concluded that the effect of percent occupancy on CO is significant.

3.3.2. Occupancy Percentage Impact towards NO₂

Table 2. Regression Analysis on Occupancy Percentage Impact towards NO₂

Predictor	β	t	R	R²	Adj. R²	F
Persen Occupancy	0.827***	8.092	0.827	0.684***	0.827	223

Note: Dependent Variable : NO₂, N= 105; ***p< .001, **p< .01 and *p< .05

The results of observations on the analysis in table 2 also show similar results. The contribution of the percent occupancy to changes in NO₂ is also quite significant (R2 = 0.64, p <0.001) or in other words the contribution of this prediction model is 68%. In addition, the results of the analysis also show that the effect of percent occupancy on NO₂ is also relatively high (β= 0.83, p < 0.001). These results indicate that the role of vehicle occupancy percentage on the road makes a rapid increase of NO₂ in the environment.

All the results of the regression analysis above show the impact of percent occupancy which consistently has an impact on air quality and noise. Based on the results of this analysis, it can be concluded that the percent of road occupancy that occurred in the four research locations can have a significant impact on changes in air quality and noise. In general, it can also be concluded that the presence of roadside parking barriers can trigger an increase in occupancy percentage, which in turn impacts air quality.

The results of this analysis then become a guide for further researchers to conduct research to examine the impact of parking changes on decreasing occupancy percent to changes in air quality and noise. Further researchers conducted a parking intervention by changing.

The results of this study emphasize that vehicles concentrating on one point of the road section caused by side barriers can worsen air quality. This means that every additional percent occupancy has the potential to also increase NO₂ and CO. Roadside parking conditions that impede vehicle movement can be one of the triggers for increased pollutant concentrations. Although this study found the impact of the position of the occupancy percentage on environmental quality, this study did not find any exhaust gas that exceeded the tolerance limit. The results of this study are in line with the findings of previous researchers regarding the impact of transportation conditions on vehicle exhaust emissions so that they affect the quality of the air people breathe [5]. Research conducted by Baumbach [20] found that several locations such as markets, bus stations, and traffic flows trigger increased concentrations of pollution due to exhaust gases such as CO and NO₂. The study also found that under certain conditions the combustion in a vehicle's engine is imperfect so that it produces far more exhaust emissions than when the vehicle is running normally.

The results of this study are in line with the researchers' initial assumption that when traffic jams occur and vehicle volume increases on a road section, at that time the occupancy percentage also increases. At the same time, vehicles are immobilized and traffic flow slows down. When this condition occurs, the combustion that occurs in

the engine becomes incomplete, resulting in more exhaust emissions that pollute air quality. Based on this explanation, a high occupancy percentage can result in the production of high exhaust emissions on roads, thereby reducing air quality. Furthermore, the spread of pollutants can also occur around the area experiencing the congestion. Based on the results of previous research, it was found that the size, shape, and variety of vehicles on the road causes the spread of pollutants to be lifted into the air and eventually spread [21]. Conditions can be exacerbated if the congestion occurs on narrow roads, especially in a tunnel [22]. The impact of this pollution does not only affect air quality but further worsens the health of the people living around the street [20].

The results of this study is in line the with previous studies [23,24] show that air quality measurements near congested roads show a significant association. At the same time, slowing the flow of vehicles increases the amount of vehicles on the road. As a result, the exhaust gases are concentrated in the same place. In addition, the combustion quality of the vehicle engine is not perfect, which eventually leads to the concentration of exhaust gases in one segment. The exhaust gases are then lifted into the air and diffused, degrading air quality [4].

Based on the findings of this study and studies from previous studies, it can be understood that there is a relationship between roadside barriers and reduced traffic speed. The slowed traffic flow then increases the occupancy percentage. The high percentage of occupancy concentrated in an area can have an impact on increasing air and noise pollution. Therefore, this study concludes that there is a strong positive relationship between roadside barriers to percent occupancy which then impacts the environment.

4. CONCLUSION

The results of this study show that there is a relationship between road barriers and reduced traffic speeds. The slower the traffic flow, the higher the occupancy. High area occupancy can increase air and noise pollution. Therefore, this study concludes that there is a strong positive relationship between roadside obstacles and occupancy affecting the environment. The high occupancy percentage as a result of the high concentration of the number of vehicles on one road has a significant contribution to environmental pollution. Environmental pollution in question is in the form of CO and NO₂ levels. The higher the occupancy percentage on the road, the higher the level of pollution due to vehicle exhaust emissions.

NOMENCLATURE

CO Carbon Monoxide
NO₂ Sodium Dioxide
VOCs Volatile Organic Compounds
GHG Greenhouse Gas

REFERENCES
[1] Sukarto, H. 2006. Urban Transport and the Environment. Journal of Civil Engineering. 3(2).
[2] Anugerah, Y., Ramli, M,I., Aly, S,H., Samang, L, 2013. Study of Road Agency Parking Systems in Tourism Shopping Areas in Makassar City. Civil Engineering National Seminar. ITS. 6th February 2013.
[3] Irawati, I.2015. Analisis Emisi Gas Buang Kendaraan Bermotor Pada Kawasan Pasar Tradisional Dengan Pendekatan Mikrosimulasi The 18th International Symposium (Bandar Lampung:Unila) pp. 929-936.
[4] Gunawan, H and Budi, S.G. 2016. Kajian Emisi Kendaraan di Persimpangan Surabaya Tengah dan Timur Serta Potensi Pengaruh Terhadap Kesehatan Lingkungan Setempat (Jurnal Wilayah dan Lingkungan vol 5) pp. 113-124.
[5] Poernomosidhi, P.I.F. (1995). "Review on Road Environment Condition and Research on Traffic Noise and Air Pollution in Indonesia", Paper for the Technical Visit to Publik Work Research Institute, Tsukuba, Japan, 25th Sept-6th Oct. 1995.
[6] Al-Momani,T.M. and A.D. Al-Nasser. 2011. Emission Rate of Gases Emitted from Private Gasoline Vehicles in Irbid – Jordan. Jordan Journal of CivilEngineering, 5(2): 287-301.
[7] Sattar Y, M. Rashid, M. Ramli and B. Sabariah., 2014. Black carbon and elemental concentration of ambient particulate matter in Makassar Indonesia. IOP Conf.Series: Earth and Environmental Science. 18. 012099: doi : 10.1088/1755-1315/18/1/012099.
[8] Sattar., M Rashid., R Mat., and L Puji., 2012. A Preliminary Survey of Air Quality in Makassar City South Sulawesi Indonesia. Jurnal Teknologi, 57: 123-136.
[9] Rashid, M., Sattar,Y., Ramli, M., Sabariah., and Puji, L.,
2014. PM10 black carbon and ionic species concentration of
urban atmospheric in Makassar of South Sulawesi Province,
Indonesia. Atmospheric Pollution Research . 5 : 610-615: doi: 10.5094/APR.2014.070.
[10] Santos G, Hannah Behrendt, Laura Maconi, Tara Shirvani dan Alexander Teytelboym. 2010. Externalities and Economic Policies in Road Transport. [Jurnal]. Research in Transportation Economics, 28: 2-45.
[11] Majumdar, D., Mukherjeea, A.K., Sen, S. 2011. BTEX
in Ambient Air of a Metropolitan City. J Environmental

Protection. 2:11-20.doi:10.4236/-jep.2011.21002.
[12] Imura H. 2003. The Budgets of GHGs, Urban Air Pollutants and Their Future Emission Scenarios in Selected Mega Cities in Asia (APN 2002-04). Final Activity Report. Air Pollution Network.
[13] WHO (World Health Organization). 2000. Air Quality
Guidelines For Europe, WHO Regional Publications, European Series, 2nd edition, Vol. 91.
[14] Banister, D., and Button, K. 1998. Transport Policy And The Environment. E & FN SPON. London.
[15] Brady, J. and O'Mahony, M. 2011. Travel to work in Dublin. The Potensial Impact of electric vehicles on climate change and urban quality. Transportation Research Part D: Transport and Environment. 16: 188-193.
[16] McNabola, A., Eyre, G.J., and Gill, L.W. 2012. Environmental tobacco smoke in designated smoking areas
in the hospitality industry: Exposure measurements, exposure modeling and poliy assessment. Environment International. 44: 68-74.
[17] Atkinson,R.W., Barratt, B., Armstrong, B., Beevers, S.D., Mudways, I.D et al. 2009. The Impact of Congestion
Charging Scheme on Air pollution Concentration in London. Atmospheric Environment. 43: 5493-5500.
[18] Roumboutsos, A., and Kapros, S.A. 2008. A Game Theory Approach to Urban Public Transport Integration Policy. Transport Policy. 15: 209-215.
[19] Saini M., Rusdi, N., Sattar, Y., Ibrahim. 2018. The Influence of Throat Length and Vacuum Pressure on Air Pollutant Filtration Using Ejectors. *AIP Conference Proceedings*.
[20] Baumbach, G,. Voght, U., Hein, K.R.G., Oluwoleb, A. F., Ogunsolab, O.J. Olaniyib, H.B., & Akeredolub, F.S.
(1995). Air Pollution in an a large troipical city with a high
traffic density – results of measurements in Lagos, Nigeria.
The Science of The Total Environment, 169, 25-3.
[21] Bautmage, U., & Gokhale, S. 2016. Effects of moving-
vehicle wakes on pollutant dispersion inside a highway road
tunnel. Environmental Pollution, 2018. 783-793. https://doi.org/10.1016/j.envpol. 2016.08.002
[22] Bari, S., and Naser, J. 2010. Simulation of airflow and pollutan level caused by severe traffic jam in a road tunnel. Tunneling and Underground Space Technology Incorporating Trenchless Technology Research, 25. 70-77. http://doi.org/10.1016/j.tust. 2009.9.04.
[23] Zhongan M and Shengan G.2002.Traffic Pollution in Xi'an City (Hongkong-Hongkong SARR).p.21
[24] Tarigan,A. 2009. Estimasi Emisi kendaraan Bermotor di Beberapa Ruas Jalan di Kota Medan. Tesis Sekolah Pasca Sarjana Universitas Sumatera Utara Medan.
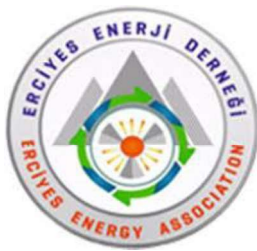
Energy, Environment and Storage
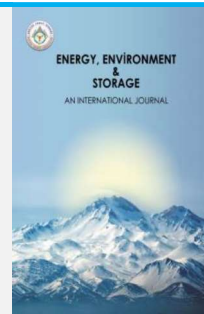
Testing of Some Ionic Liquids at the Synthesis of Biodiesel

Ibrahim Mamedov[1], Mahmud Musazade[2], Hurupari Rustamova[3],

Ofelia Javadova[4], Nargiz Azimova[5]

[1]*Baku State University, Baku, Azerbaijan, ORCID: 0000-0002-5757-9899*

ABSTRACT. The aim of the present work was to the preparation of biodiesel from sunflower oil and methanol by the transesterification reaction in the presence of some ionic liquid catalysts. The yield was 98% using a 1:5 molar ratio of oil to alcohol at 55°C and in the quinoline-based ionic liquid catalyst. Important fuel exploitation properties of B20 and B50 fuel blends have been investigated. The obtained results showed that B20 and B50 blends have a greater advantage for diesel engines than B100 and fossil diesel fuels. The best results were demonstrated B20 fuel blend among the studied fuels.

Keywords: Transesterification, Biofuel, Biodiesel, Ionic Liquid, Catalyst

1. INTRODUCTION

The promising and dynamic developing area of research in the field of biofuel production is the technology for producing biodiesel, which has a lot of significant advantages compared to petroleum products and other fossil fuels. The volume of biofuel production in the world is increasing on a large scale. If in 2021 the share of biofuels in the world production of fuel for road transport was 3.6%, then the International Energy Agency (IEA) predicts its increase to 15% by 2030 [1-8].

From the alternative type of fuels, biodiesel is a renewable resource consisting of fatty acid alkyl monoesters derived from vegetable oil, waste animal fats, waste cooking oil, etc. It is important to note that the combustion of biodiesel does not emit toxic substances that cause environmental problems due to the absence of aromatic, nitrogenous, and sulfurous compounds. According to a review of emission data for heavy-duty engines published by EPA (Environmental Protection Agency of USA 2002), from diesel to B20, carbon monoxide, toxic hydrocarbons, and particle matter decreased by 13, 20 and 20 % respectively [9-15].

The production of biodiesel is mainly based on the FAME formation reaction. The transesterification reaction can be catalyzed by homogeneous alkali catalysts such as sodium hydroxide, sodium methoxide and potassium hydroxide or homogeneous acid catalysts such as sulfuric acid or hydrochloric acid, ionic liquids, etc. [16-17].

Considering the above, in the presented work, the transesterification reaction of sunflower oil with methyl alcohol in the presence of pyridine and quinoline based ionic liquid catalysts at first was carried out. The important exploitation properties of B20 and B50 fuel blends were estimated.

2. MATERIALS AND METHODS

All the chemicals for the synthesis of ionic liquids and biodiesel were obtained from commercial sources (Aldrich) and used as received (Figure 1, 2).

Samples of diesel fuel, sunflower oil were purchased at a fuel station and markets in Baku, Azerbaijan. The B20 and B50 fuel blends were prepared by mixing diesel and biodiesel by volume (B20- 20% biodiesel and 80% diesel; B50- 50% biodiesel and 50% diesel).

NMR experiments have been performed on a BRUKER FT NMR spectrometer (UltraShieldTM Magnet) AVANCE 300 (300.130 MHz for ^{1}H and 75.468 MHz for ^{13}C) with a BVT 3200 variable temperature unit in 5 mm sample tubes using Bruker Standard software (TopSpin 3.1). The ^{1}H and ^{13}C chemical shifts were referenced to internal tetramethylsilane (TMS); the experimental parameters for ^{1}H: digital resolution = 0.23 Hz, SWH = 7530 Hz, TD = 32 K, SI = 16 K, 90^0 pulse-length = 10 µs, PL1 = 3 dB, ns-= 1, ds= 0, d1 =1 s; for ^{13}C: digital resolution = 0.27 Hz, SWH = 17985 Hz, TD = 64 K, SI = 32 K, 90^0 pulse-length = 9 µs, PL1 = 1.5 dB, ns= 100, ds= 2, d1= 3 s. NMR-grade $CDCl_3$ was used for the analysis of ethylene glycol ketal and fuel blends.

*Corresponding author: bsu.nmrlab@gmail.com

Fig. 1. The chemicals for the synthesis of ionic liquids


Fig. 2. The preparation of the ionic liquids

Preparation of 2-(triethyl-λ^4-azanyl)ethan-1-ol chloride (TAEC).

An equimolar amount of the triethylamine and *2-chloroethanol* were dissolved in ethanol and the solution was kept under vigorous stirring at 70ºC for 24 hours. After cooling to room temperature, ethanol was evaporated from the mixture to give a basic TAEC ionic liquid catalyst.
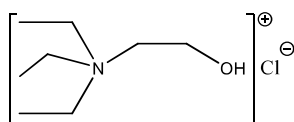
*Preparation of 4-bromophenacyl pyridinium hydroxide (BPPH).*

An equimolar amount of 4-bromophenacylpyridinium bromide and KOH was dissolved in ethanol and the solution was kept under vigorous stirring at 70ºC for 24 h. After cooling to room temperature, KBr was removed by filtration and ethanol was evaporated from the mixture to give a basic BPPH ionic liquid catalyst.
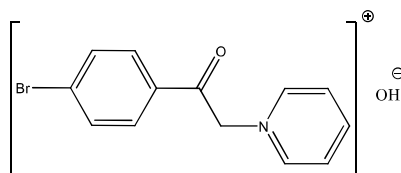
Preparation of 4-bromophenacyl quinolinium hydroxide (BPQH).

An equimolar amount of 4-bromophenacylquinolinium bromide and KOH was dissolved in ethanol and the solution was kept under vigorous stirring at 70ºC for 24 h.

After cooling to room temperature, KBr was removed by filtration and ethanol was evaporated from the mixture to give a basic ionic liquid catalyst BPQH.
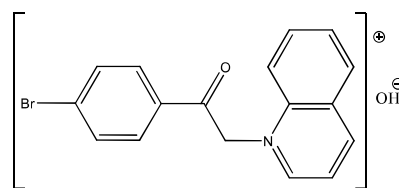
The procedure for the preparation of biodiesel

Sunflower biodiesel (B100) was synthesized by dissolving 0.5 g of BPPH (BPQH or TAEC) in 35 ml of methanol (CH_3OH) without heating at room temperature (Figure 3). After complete dissolution, 100 ml of oil was added to this mixture. The reaction was carried out in a conical flask equipped with a reverse refrigerator and magnetic stirrer for 6 hours at 55ºC. After stirring, the reaction mass was aged for at least 12 hours in a dividing funnel. The reaction mass was divided into two layers using a dividing funnel: the upper layer contained biodiesel and the lower layer glycerine. Untreated biodiesel was repeatedly washed with hot distilled water to remove catalysts. Water removal is achieved by distillation.

The yield of biodiesel was 83% and 98% when used the molar ratio of oil to methanol 1:5, as catalyst accordingly BPPH and BPQH.
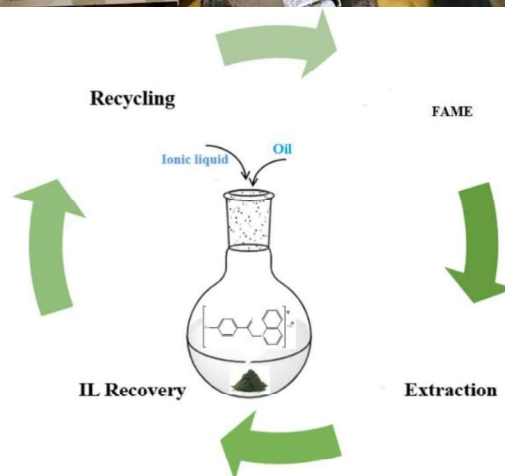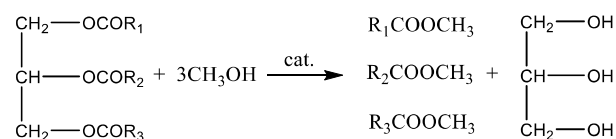
Fig. 3. The preparation of the biodiesel

Biodiesel synthesized from sunflower oil and its blends were characterized by the American Standard of Testing and Materials (ASTM) methods.

3. RESULTS AND DİSCUSSİON

In our previous works [11-15], the preparation of methanol, and ethanol biodiesels catalyzed by a different catalytic system and testing of their exploitation properties had been informed.

In recent years, a new biomass processing technology using ionic liquid (IL) has been developed for the production of biofuels. Despite the high cost of ionic liquid catalysts, their main advantage is reuse and simple cleaning process [18-19].

This work is devoted to the preparation of methanol biodiesel from the sunflower oil at presence of some ionic liquid systems and testing of their different exploitation properties.

The used sunflower oil physicochemical properties are shown in Table 1.

Table 1 Major fatty acids and physical properties of the refined sunflower oil

Fatty acid composition (wt.%)	16:0	18:0	18:1	18:2
	3.5–7.6	1.3–6.5	14–43	44–74
Acid value (mg of KOH/g)	0.28±0.5			
Saponification value (mg KOH/g)	193.3±0.5			
Iodine value (g I_2 per 100 g)	121.4±0.5			
Viscosity (cP)	34.1±0.5			
Flash point (°C)	265			
Pour point (°C)	+12			
Density (g/cm³)	0.9186			

At studying of biodiesel synthesis process in the presence of TEAC, it was determined that the catalyst is inactive in the transesterification reaction. However, as a result of our studies, it was demonstrated that TEAC catalyst is active in the alkylation reaction of toluene with 2-chloroethanol.
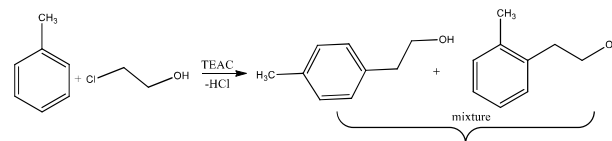
The yield of biodiesel was 83% at using the molar ratio of oil to methanol 1:5, as catalyst BPPH.

To increase the size of the cation in the ionic liquid, quinoline was used in the synthesis of the catalyst. The biodiesel yield was 98% using a 1:5 molar ratio of oil to methanol as the BPQH catalyst. Below is the given mechanism of the formation of biodiesel in the presence of an ionic liquid catalyst.
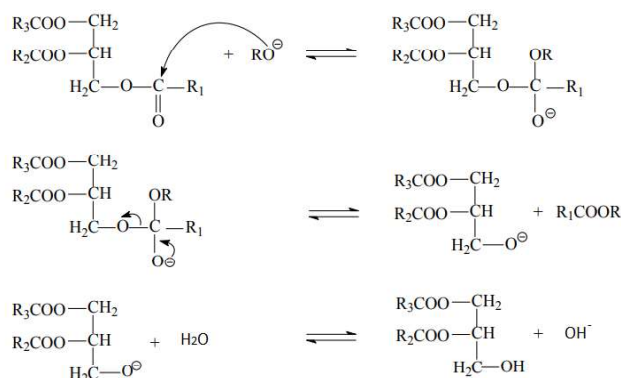
Fig. 4. Mechanisms of the transesterification in the presence of ionic liquid

Table 2 The exploitation properties of B10, B20, B100 and diesel fuels

| Properties	ASTM Methods	ASTM diesel	ASTM biodiesel	diesel	B20	B50	B100
Relative density at 20°C, g/cm³	D1298	0.8-0.84	0.86-0.9	0.837	0.859	0.864	0.88
Viscosity at 40°C, mm²/s, min-max.	D445	2-5	3.5-5.0	3.44	3.60	3.78	4.1
Flash point, °C, min.	D93	65	>120	70	105	119	174
Cloud point (°C)	D2500	-12	<20	+7	+5	+10	+12
Pour point (°C)	D2500	-15	<15	0	-5	+3	+6
Iodine value g (l_2)/100 g	-	60-135	<120	1.58	45.7	88.9	110.5
Sulfur, ppm, max.	D 975-14	15	15	50	33	27	0
Water and sediment, vol%, max.	D 975-14	0.05	0.05	0	0	0	0
Copper corrosion, 3 hr at 50°C, max.	D 975-14	№3	№3	№2	№1	№1	№1
Cetane number, min.	D 975-14	40	47	43.4	44.1	45.6	48.5

As noted above, in recent years acidic and basic IL systems have been used for the synthesis of biodiesel. In most basic ILs, a substrate with a small free fatty acids (FFA) content is required to evade soap formation. The presented work catalytic activity of triethylamine (TEAC), pyridine (BPPH) and quinoline (BPQH) based ILs have been investigated.

In the continuation of the investigations, the properties of B20 and B50 fuel blends were studied. The exploitation properties of the diesel, sunflower biodiesel (B100), B20, and B50 blends were investigated and the results are shown in Table 2.

As seen in Table 2 density increased for B20 and B50 fuel blends. The density is a factor governing the quality of

crude petroleum, but it is an uncertain indication of petroleum product quality unless correlated with other properties. According to the good afreement between the density and viscosity, kinematic viscosity also insignificantly increases as the percentage of biodiesel in the blends, but it is in the ASTM limit of 2-5 at 40°C.

The flash points are increased for the B20 and B50 blends than diesel fuel. It is also observed that flash points of pure biodiesels were higher than those of diesel and indicated blends. In this case, the biodiesel blends are hard to ignite with a higher flash point. But increasing flash point implies safer handling and storage.

The amount of sulfur significantly decreased as the percentage of biodiesel blends from 50 up to 27 ppm, which is very important for the environment and human health. As shown in our experimental results, water, sediment, also copper corrosion parameters are excellent.

Considering the above indicated, we note that B20 and B50 fuel blends have high potential as an ecological pure fuel than simple diesel fuel.

The reported work was informed the new İLs catalytic systems, which have a positive influence on biodiesel production, and separation processes and it can be reused.

4. CONCLUSIONS

The presented work reported the application possibility of a new basic İLs catalytic system at the transesterification process. High yield (98%) was observed in the quinoline-based ionic liquid catalyst, but the triethylamine-based catalyst is active in the alkylation reaction of toluene with 2-chloroethanol.

The properties of diesel, sunflower biodiesel B20 and B50 blends were investigated on the ASTM standards. The best exploitation properties were demonstrated B20 fuel blend among the studied fuels.

REFERENCES

[1] Edirin, B. A., Nosa, A. O. A comprehensive review of biomass resources and biofuels production potential in Nigeria, *RJEAS*, 1(3), 149-155, 2012.

[2] Niju, S., Anushya, C., Balajii, M. Process optimization for biodiesel production from Moringa oleifera oil using conch shells as heterogeneous catalyst, *Environment. Program. on Sustainab. Energy*, 38, 1-14, 2019.

[3] Selvaraj, R., Praveenkumar, R., Moorthy, I. G. A comprehensive review of biodiesel production methods from various feedstocks, *Biofuels*, 10, 325-333, 2019.

[4] Aransiola E. F., Ojumu, T. V., Oyekola, O. O. A review of current technology for biodiesel production: state of the art, *Biomass Bioenergy*, 61, 276-297, 2014.

[5] https://www.iea.org/reports/biofuels

[6] Zheng, M, Mulenga, M.C., Reader, G.T., Tan, Y., Wang, M., Tjong, J. Neat biodiesel fuel engine tests and preliminary modeling, *SAE Technical Paper Series*, 01, 1-16, 2007.

[7] Nwafor, O.M.I. Emission characteristics of diesel engine operating on rapeseed methyl ester, *Renew. Enerergy*. 29, 119-129, 2004.

[8] Prasad, T.H., Reddy, K.H.C., Rao, M.M. Performance and exhaust emissions analysis of a diesel engine using methyl ester of oil with artificial neural network aid, *Inter. J. Engineer. Tech.*, 2, 23-27, 2010.

[9] Environmental Protection Agency of USA (2002) A comprehensive analysis of biodiesel impacts on exhaust emissions. Draft technical report (EPA420-P-02-001) web. https://19january2017snapshot.epa.gov/www3/otaq/models/analysis/biodsl/p02001.pdf).

[10] Shahmirzae, H.J., Fallahipanah, M., Hashemi M. G., Chen, L. Performance analysis of Diesel engines fueled by biodiesel blends via thermodynamic simulation of an air-standard diesel cycle, *Int. J. Environ. Sci. Technol.*, 11, 139-148, 2014.

[11] Mamedov, I., Huseynova, S., Javadova, O., Azimova, N. Pine oil and glycerol ketal as components of B10 fuel blends, *Indian Journal of Chemical Technology*, 29, 442-447, 2022.

[12] Mamedov, I., Huseynova, S., Javadova, O., Azimova, N., Huseynova, R., Gasimova, Sh, Testing of pine oil and glycerol ketal as components of B10 fuel blend, *Energy, Environment and Storage*, 2(1), 11-14, 2022.

[13] Mamedov, I., Mamedova, G., Azimova, N. Testing of ethylene glycol ketal, dioxane and cyclopentanone as components of B10, B20 fuel blends, *Energy, Environment and Storage*, 2(3), 9-12, 2022.

[14] Guliyev, S., Mamedov, I.G. UV irradiation testing of biodiesel from the Alhagi oil and diesel-biodiesel mixtures, *Proc. Univer. Appl. Chem. Biotech.*, 3, 455-461, 2022.

[15] Mamedov, I.G., Javadova, O.N., Azimova, N.V. Preparation of diesel fuel blends and study of their physical properties, *Proc. Univer. Appl. Chem. Biotech.*, 2, 332-338, 2020.

[16] Lee, H.V., Juan, J.C., Taufiq-Yap, Y.H., Kong, P.C., Rahman, N.A. Advancement in heterogeneous base catalyzed technology: An efficient production of biodiesel fuels, *J. Renew. Sust. Energy*, 7, 1-47, 2015.

[17] Amin, T.K., Amin, N.A.S., Hossein, M. A review on novel processes of biodiesel production from waste cooking oil, *Appl. Ener.*, 104, 683-710, 2013.

[18] Han, B., Zhang, W., Yin, F., Liu, S., Zhao, X., Liu, J., Wang, C., Yang, H. Optimization and kinetic study of methyl laurate synthesis using ionic liquid [Hnmp]HSO4 as a catalyst, *R. Soc. open sci.* 5, 180672, 1-16, 2018.

[19] Bin, J., Yumei, W., Luhong, Z., Yongli, Sun., Huawei, Y., Baoyu, W., Na Y. Biodiesel Production via transesterification of soybean oil catalyzed by superhydrophobic porous poly(ionic liquid) solid base, *Energy Fuels*, 31(5), 5203–5214, 2017.
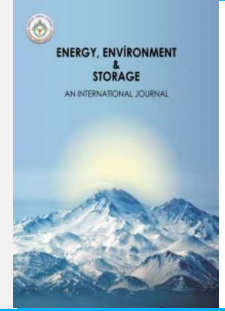
Climate Change and Animal Movement Integration in the Environmental Niche Model

Halil Emre Kislioglu[1,2], Ivan Vera [2], Giacomo Di Lallo [2], Riki Hissink[2]

[1]*Suleyman Demirel University, Department of Environmental Engineering ORCID: 0000-0002-1852-6970*

[2]*Utrecht University, Faculty of Geosciences*

ABSTRACT. Changing precipitation and temperature patterns due to climate change, shift ecological niches which pose a challenge for species. Furthermore, it is still unclear that if climate change faster than the speed of the species to move to more suitable environments. Climate Envelope models (GEMs) are used extensively in this matter to predict species geographical distribution. In this study, climate data and animal movement strategies integrated into the environmental niche model to analyze the successes of the species that have different movement strategies under the changing climate conditions. Four different movement strategies are formulized; lazy knowledge strategy (LKS), lazy no knowledge strategy (LNKS), proactive knowledge (PKS) and proactive no knowledge strategy (PNKS). In this study, mean annual temperature and annual precipitation data gathered for the RCP8.5 scenario from the HadGEM2-ES GCM model at a 10-minute resolution. Results show that the PKS has the highest survival rates which makes it the most successful strategy. Furthermore, the species with knowledge had performed higher survival rates than the species without knowledge due to their skill to find the most suitable cells around them. One-Way Anova test confirmed that there are significant differences between the strategies. Moreover, the analysis suggests that the species with knowledge of their environment have the most successful strategies for facing the climate change.

1. INTRODUCTION

Climate Envelope Models (CEMs) have been commonly used to predict species geographical distribution depending on their environmental necessities (Hijmans and Graham, 2006). Distribution of species is being affected by climate change, however changes in dispersion can vary substantially by species (Prevey et al., 2020;Smithers et al.,2018). The expected climatic changes will represent a demanding challenge for species to find a suitable environment, resulting in possible distributions shifts. In fact, in numerous studies, it is suggested that global climate change will cause species to move to more suitable locations (Chen at al., 2011; Ehrlén & Morris, 2015; Kelly & Goulden, 2008; Lenoir at al., 2008; Parmesan & Yohe, 2003). Miller and Holloway (2015) have highlighted the importance of including real data in species movement patterns, especially for future distributions projections ruled by climate change. Additionally, species movement may also be influenced by their biology and by interaction with the environment and other species. Different studies such as Stanton et al. (2015) affirm that species will have to traverse extensive landscapes to cope with climate change

which could result in species extinction. Also, in recent years a many studies investigated how climate change effect species by using climate projections (Adde et al., 2020; Baisero et al., 2020; Hosni et al., 2020) Furthermore, climate change may be faster than the ability of species to move to more suitable environments (IPCC, 2014), and may be a driver of species extinction. The success of these distribution projections are still unclear (Hijmans &Graham, 2006), several important variables (species movement) need to be included to obtain more advance future scenarios. The purpose of this research is to understand how different species movement patterns in combination with environmental suitability may affect species distribution projections. Based on the purpose of the study, this research aims to acknowledge how will 4 different movement strategies in combination with environmental suitability (mean annual temperature and annual precipitation) affect species distribution projections for the RCP 8.5 scenario.

*Corresponding author: emrekslgl@gmail.com

2. MATERIALS AND METHODS

In this research, the Matlab modelling tool was used to combine the Environmental Niche model and the Cellular Automata model to implement more realistic species movement based on the climatic suitability. The climatic suitability is dependent on the change of 2 climatic variables; annual mean temperature and annual precipitation. The implementation of movement into the Niche model will enable the visualization of the change of species distribution over time based on initial distribution rather than probability.

2.1 Bioclimatic variables and time steps

The data on the Annual Mean Temperature and the Annual Precipitation was gathered from WorldClim for the period ~1950-2000 (current conditions) and the year 2050 (average 2041-2060) and the year 2070 (average for 2061-2080) (WorldClim, 2016.). For the current condition, the middle value of the years (~1950-2000) was selected (1975) to be the starting year for our model run. The values for the bioclimatic variables; Mean Annual Temperature and Annual Precipitation were gathered for the RCP8.5 scenario from the HadGEM2-ES GCM model at a 10-minute resolution. The reason for selecting the RCP8.5 scenario is that the changes in precipitation and temperature will be large and hence will lead to a larger effect on the movement and distribution of the species. The modelled time period is 1975-2050 and 2050-2070. Since movement is dynamic through time, annual values for the bioclimatic variables were required rather than snapshot values at 1975, 2050 and 2070. Therefore, a linear relationship was used to interpolate the values of the two climatic variables for the years from 1976 to 2049 and from 2050 to 2069. This resulted in values for the climate variables for each time step for the period of 1975-2070. By using these values, it becomes possible to apply movement to the distribution, hence show the changes in distribution over time due to climate change.

2.2 The species and its initial distribution

The species used for this research are fictive species and is therefore not based on real data. The reason for choosing a fictive species is that this research focuses on the influence of different movement patterns on the distribution of a species under changing climate conditions; it is irrelevant what the exact species is. The initial distribution of species is located around the equator since the cell size varies little in comparison to cells closer to the poles. The gauss function was used to establish the combined suitability of every cell for the species for the two climatic variables. For temperature, the optimum (mu) was set to 25 degrees Celsius with a sigma value of 5 to model a species sensitive to temperature which lives in the tropical forest around the equator. For precipitation, a mu of 1800mm and a sigma of 100 was used to place the species in the wet climate of the tropics. To establish the initial (equilibrium) distribution the suitability was used; every cell where the suitability in 1975 was higher than 0.8 one individual was placed. This resulted in an initial distribution of 4966 individuals around the equator, mainly in Brazil, Africa and Indonesia. For this research, the focus was on the distribution in the tropics in Central Africa since the density was adequate for visualization.

2.3 Movement

The species is assumed to move only one cell each time step to one of the 8 neighboring cells. Four different movement strategies were created to simulate how the way a species moves affects its survival and distribution under changing climate conditions. The movement strategies are based on two different scalars; no knowledge / knowledge and lazy / proactive. Knowledge means the species has knowledge about the suitability of the neighboring cells and the species will therefore only move to cells suitable than the one it is currently located in. No Knowledge means the species has no knowledge about the suitability of the neighboring cells. Lazy means the species prefers to stay in its current cell as long as it is suitable, because of attachment to its current environment. Proactive means the species prefers to roam around annually. Below the four different are described.

2.3.1 The Lazy Knowledge strategy (LKS)

Species with the LKS strategy have the characteristic of moving only to cells that have better suitability than the one they are currently located, because they have knowledge of the suitability values from their neighboring cells (Figure 1). There are two types of rules that drive this strategy. If the local suitability is high, the species has a low probability to move, and vice versa. If the species does decide to move, it will evaluate the environmental suitability of the neighboring cells. If there are no neighboring cells with a higher suitability, the species will stay in its current cell. If there are neighbors with higher suitability values, the species will move with a probability condition; if the probability condition is met, the species choose randomly to which cell to move. If the probability condition is not met, the species remains in its current cell. The species that uses this strategy have a high inclination of saying in their cell if it is suitable.
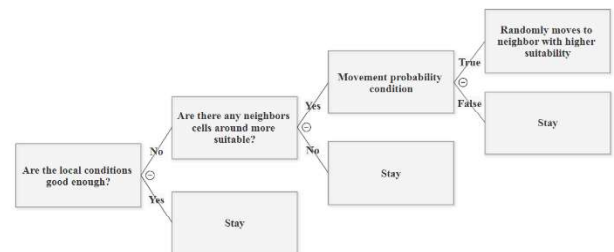

Fig. 1. The decision tree for the movement strategy Lazy Knowledge Strategy (LKS)

2.3.2 The Lazy No Knowledge strategy (LNKS)

The LNKS is similar to the LKS. The main difference is that this strategy does not have knowledge of the suitability of the surrounding cells. If the suitability of the local cell is low, the species has a high probability to move randomly to a neighboring cell, and vice versa, without taking into account the suitability of the cell it moves to (Figure 2).
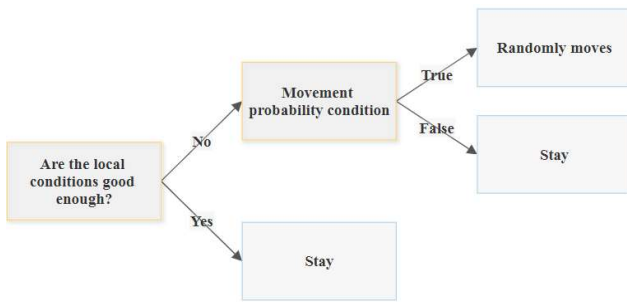
Fig. 2. The decision tree for the movement strategy Lazy No-Knowledge Strategy (LNKS)

2.3.3 The Proactive knowledge Strategy (PKS)

The PKS knows the suitability of their neighboring cells, just like the LKS. If the suitability of the neighboring cells is lower than the suitability of the current cell, the species will remain in the current cell. If the suitability values of the neighboring cells are higher, the species has a probability to move to every neighboring cell. If the probability condition is met, the species will randomly move to any neighbor with a higher suitability (Figure 3). This movement strategy has a higher chance of movement than the LKS, hence it is proactive.
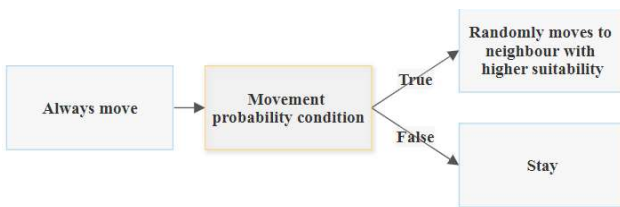

Fig. 3. The decision tree for the movement strategy Proactive Knowledge Strategy (PKS)

2.3.4 The Proactive No Knowledge Strategy (PNKS)

The PNKS is the simplest strategy; the species will randomly move to a neighbor every year. The species has no knowledge about the suitability of the neighboring cells; the movement is driven by randomness and is therefore similar to dispersal (Figure 4).
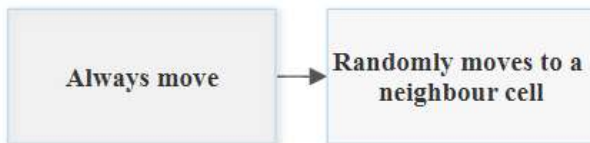
Fig. 4. The decision tree for the movement strategy proactive no knowledge (PNKS)

2.4 Movement Rules

Extinction due to climate conditions was added to the model to make sure that individuals living under unsuitable conditions would not survive since this would give unrealistic distributions. However, even at high suitability extinction due to climate conditions can happen due to local conditions, albeit at a low rate. There a mathematical function was introduced that will have a high probability of extinction at low suitability values and a low probability of extinction at high suitability values (Figure 5): the Probability to go extinct = $1 * \exp(-10. * \text{Suitability of the Cell})$. By making the function an exponential decline function, the extinction probability is low for a suitability of >0.5. Below 0.5 the chance to go extinct increases

exponentially to a probability of 1 at a suitability of 0. This extinction probability is included for all movement strategies.
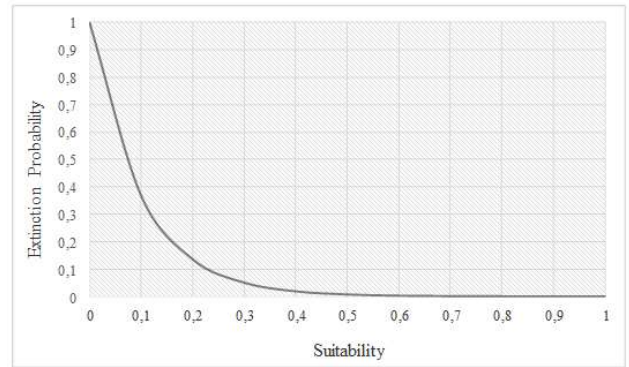

Fig. 5. The visualization of the extinction formula, probability to go extinct = $1 * \exp(-10 * \text{Suitability})$

2.5 Statistical analysis

A One-way Anova test was performed to determine if there were any statistical differences between movement strategies in relation with number of individuals and cells occupied. A Shapiro Wilk test was performed to identify if variables were normally distributed. Additionally, a Levene's test was used to check for homoscedasticity.

3. RESULTS

The spatial distribution of the species for the four different movement strategies is shown in figure 6. It is obvious that the PNKS strategy is least successful, both in individual numbers and the extent of its distribution. However, for the strategies, the differences are less clear. The results of the statistical tests are discussed below to distinguish between the success of the various movement strategies.
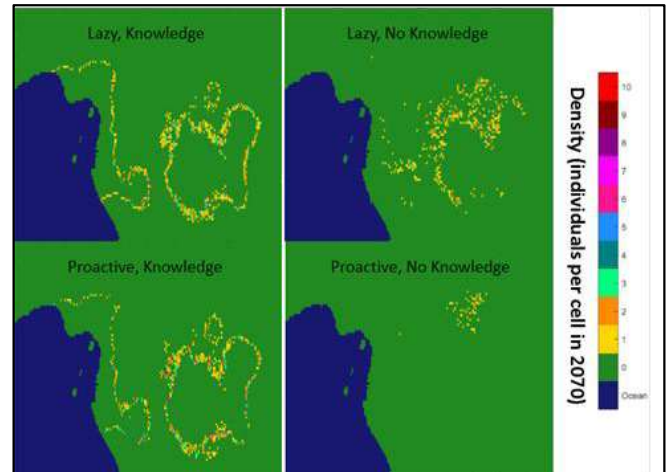

Fig. 6. The distribution maps in 2070 for the four different movement strategies in Central Africa

The results of the model indicate that the PKS is the best strategy for species to survive under the RCP 8.5 scenario. The species with knowledge had a better survival performance than the species without knowledge (Figure 7). For each strategy, different distributions were observed (Figure 6); the species with knowledge tend to congregate together in highly suitable cells while the species who do not have knowledge disperse and experience higher

extinction rates. There is a considerable decrease in populations by 2070 for LNKS and PNKS by 78.7% and 98.6% respectively. On the other hand, the LKS and PKS performed better by 35.6% and 40% decrease in population respectively. The One Way Anova test confirmed that there are strong significant differences between all groups (p=0.00).
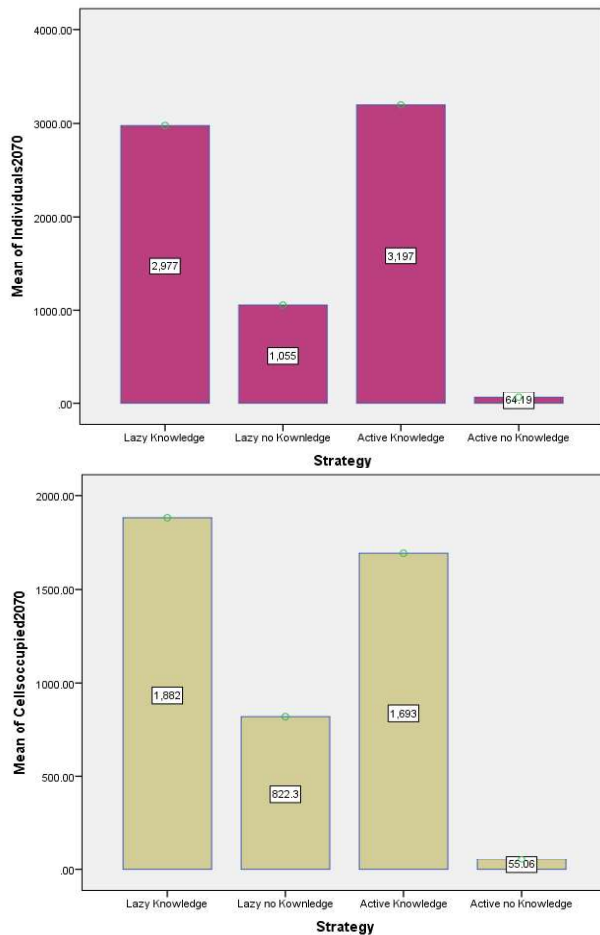

Fig. 7. The mean amount of individuals that survived in 2070 (top) and the mean amount of cells occupied (n=33 runs) in 2070 for the four different movement strategies (bottom).

Regarding occupied cells, the Anova tests also confirmed significant differences between strategies (p=0.00). The PKS is the strategy with most cells occupied in 2070, followed by LKS, LNKS and PNKS (figure 7). The occupied cells results are consistent with the number of individual alive in 2070, showing the strategies with more individuals alive are also the ones with more occupied cells due to high number of individuals.

4. CONCLUSIONS

The study suggests species with knowledge of their environment have the most suitable strategy for facing climate change. On the other hand, even if strategies are significantly different (p=0.00), the LKS strategy leads to a high number of surviving individuals in 2070 compared to the no knowledge strategies. The clustering of the PKS may seem to be a good strategy to face climate change. However, the model does not take into account the interaction between individuals (competition) or any sort of carrying capacity. Therefore high densities of individuals in one cell are unlikely to occur in reality, although this is also partially dependent on the characteristics of the species. This assumption, and the lack of adaptation, stem from the original Niche model.

Different assumptions might have influenced strategies movement. The model assumed species could only move one cell per year in eight directions. In reality, the step size is dependent on the characteristics of the species and therefore could potentially be smaller or larger than one cell. The model used a fictive species with an equilibrium distribution located around the equator, since the cell sizes in this region are similar. The rule of moving one cell per year is more valid than for areas closer to the poles where the differences in cell size are larger. The movement strategies fit within a simple version of the Lagrangian approach applied to the Niche model (Smouse et al., 2010).

Another assumption is based on the climatic parameters and data. The model only used two climatic parameters (annual mean temperature and annual precipitation), whereas other climatic factors may also have influenced species movement projections. The available data was limited to only three averages in time and linear changes in mean annual temperature and annual precipitation around the globe was assumed to be able to model annual distribution changes. Natural movement barriers such as lakes and rivers, and anthropogenic structures such as city, roads and towns were also not taken into account.

This model included different strategies that species may use to compensate with climate change projections. However, further research may include real data and species behavior to have a better understanding of how climate change will relate to species movement and extinction.

REFERENCES

[1] Chen, I.-C., Hill, J. K., Ohlemuller, R., Roy, D. B., & Thomas, C. D. (2011). Rapid Range Shifts of Species Associated with High Levels of Climate Warming. Science, 333(6045), 1024–1026. https://doi.org/10.1126/science.1206432

[2] Ehrlén, J., & Morris, W. F. (2015). Predicting changes in the distribution and abundance of species under environmental change. Ecology Letters, 18(3), 303–314. https://doi.org/10.1111/ele.12410

[3] Hijmans, R. J., Graham, C.H., C. H. (2006). The ability of climate envelope models to predict the effect of climate change on species distributions. Global Change Biology, 12(12), 2272–2281. https://doi.org/10.1111/j.1365-2486.2006.01256.x

[4] Kelly, A. E., & Goulden, M. L. (2008). Rapid shifts in plant distribution with recent climate change. Proceedings of the National Academy of Sciences, 105(33), 11823–11826. https://doi.org/10.1073/pnas.0802891105

[5] Lenoir, J., Gegout, J. C., Marquet, P. A., de Ruffray, P., & Brisse, H. (2008). A Significant Upward Shift in Plant Species Optimum Elevation During the 20th Century. Science, 320(5884), 1768–1771. https://doi.org/10.1126/science.1156831

[6] Miller, J. A., & Holloway, P. (2015). Incorporating movement in species distribution models. Progress in Physical Geography: Earth and Environment, 39(6), 837–849. https://doi.org/10.1177/0309133315580890

[7] Parmesan, C., & Yohe, G. (2003). A globally coherent fingerprint of climate change impacts across natural systems. Nature, 421(6918), 37–42. https://doi.org/10.1038/nature01286

[8] Smouse, P. E., Focardi, S., Moorcroft, P. R., Kie, J. G., Forester, J. D., & Morales, J. M. (2010). Stochastic modelling of animal movement. Philosophical Transactions of the Royal Society B: Biological Sciences, 365(1550), 2201–2211. https://doi.org/10.1098/rstb.2010.0078

[9] Stanton, J. C., Shoemaker, K. T., Pearson, R. G., & Akçakaya, H. R. (2014). Warning times for species extinctions due to climate change. Global Change Biology, 21(3), 1066–1077. https://doi.org/10.1111/gcb.12721

[10] IPCC, (2014): Summary for policymakers. In: Climate Change 2014: Impacts,Adaptation,and Vulnerability. Part A: Global and Sectoral Aspects. Contribution of Working Group II to the Fifth Assessment Report of the Intergovernmental Panel on Climate Change [Field, C.B., V.R. Barros, D.J. Dokken, K.J. Mach, M.D. Mastrandrea, T.E. Bilir, M. Chatterjee, K.L. Ebi, Y.O. Estrada, R.C. Genova, B. Girma, E.S. Kissel, A.N. Levy, S. MacCracken, P.R. Mastrandrea, and L.L.White (eds.)]. Cambridge University Press, Cambridge, United Kingdom and New York, NY, USA, p. 14.

[11] Prevéy, J. S., Parker, L. E., Harrington, C. A., Lamb, C. T., & Proctor, M. F. (2020). Climate change shifts in habitat suitability and phenology of Huckleberry (Vaccinium membranaceum). Agricultural and Forest Meteorology, 280, 107803. https://doi.org/10.1016/j.agrformet.2019.107803

[12] Smithers, B. V., North, M. P., Millar, C. I., & Latimer, A. M. (2017). Leap Frog in slow motion: Divergent responses of tree species and life stages to climatic warming in Great Basin subalpine forests. Global Change Biology, 24(2). https://doi.org/10.1111/gcb.13881

[13] Adde, A., Stralberg, D., Logan, T., Lepage, C., Cumming, S., & Darveau, M. (2020). Projected effects of climate change on the distribution and abundance of breeding waterfowl in eastern Canada. Climatic Change, 162(4), 2339–2358. https://doi.org/10.1007/s10584-020-02829-9

[14] Baisero, D., Visconti, P., Pacifici, M., Cimatti, M., & Rondinini, C. (2020). Projected global loss of mammal habitat due to land-use and climate change. One Earth, 2(6), 578–585. https://doi.org/10.1016/j.oneear.2020.05.015

[15] Hosni, E. M., Nasser, M. G., Al-Ashaal, S. A., Rady, M. H., & Kenawy, M. A. (2020). Modeling current and future global distribution of Chrysomya Bezziana under changing climate. Scientific Reports, 10(1). https://doi.org/10.1038/s41598-020-61962-8

[16] WorldClim (n.d.) WorldClim - Global Climate Data. Retrieved from http://www.worldclim.com/download at 5th of January 2016 http://www.landmarkgoc.com/biogas_project.html. Accessed on 3 March 2012

Founded in 2016, our association is open to everyone who is interested in energy and devoted to sustainability.

ERCIYES ENERGY ASSOCIATION